# *Wind* 2017 Senior Review Proposal

**Lynn B. Wilson III**
NASA GSFC
Project Scientist

## Executive Summary

NASA launched the *Wind* spacecraft in November, 1994 to the Earth's L1 Lagrange point as the interplanetary component of the Global Geospace Science (GGS) Program within the International Solar Terrestrial Physics (ISTP) program. The spin stabilized spacecraft – spin axis aligned with ecliptic south – carries eight instrument suites that provide comprehensive measurements of thermal to solar energetic particles, quasi-static fields to high frequency radio waves, and $\gamma$-rays. All instrument suites continue to provide valuable scientific observations completely available to the public (except TGRS, now without coolant).

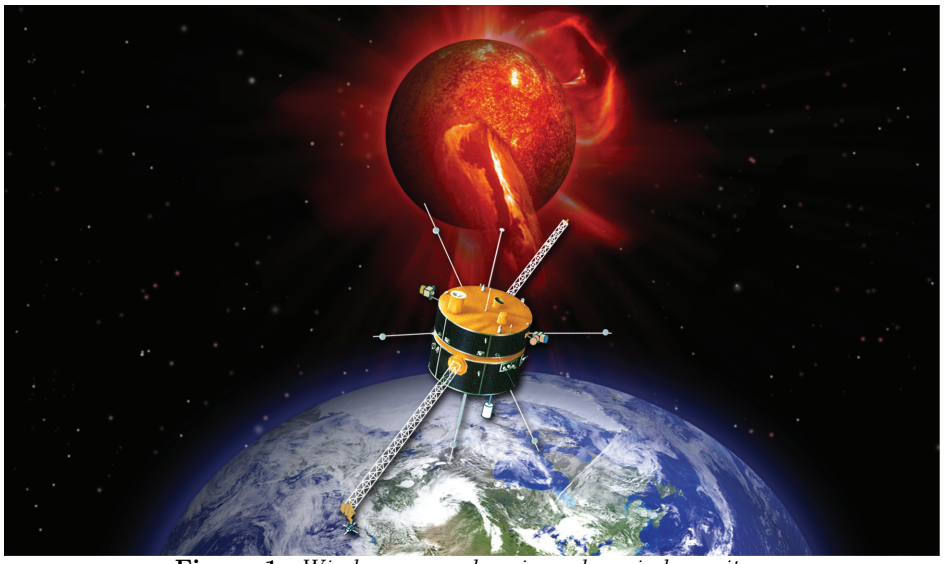

**Figure 1:** *Wind, a comprehensive solar wind monitor.*

The *Wind* instrument suite provides comprehensive and unique high time resolution (HTR) in-situ solar wind measurements that enable the investigation of wave-particle interactions. *Wind* is the only near-Earth spacecraft equipped with radio waves instrumentation. *Wind* has made numerous independent discoveries since the last Senior Review, from kinetic effects of solar wind reconnection and plasmas to solar cycle seasonal variations. *Wind* remains very active as evidenced by the **over 600 refereed publications in 2015-2017** (**over 4300 refereed publications since launch**, listed on the *Wind* project Web page: https://wind.nasa.gov), 13 doctoral and 3 Masters degrees (86 total graduate degrees since 1994), and 16 currently in progress. The new results span all three heliophysics research objectives as described in the *2014 Science Plan for NASA's Science Mission Directorate*. The *Wind* science data products are publicly served directly from the instrument team sites and CDAWeb, with a single project webpage containing links to and descriptions of the large number of *Wind* data products. *Wind* is also an active participant in the development of the Virtual Heliophysics Observatory (VHO) that allows for more complex queries than CDAWeb.

Even though *Wind* is >22 years old, the spacecraft is still in good health. *Wind* continues to remain an active mission as evidenced by the >1,825,000 data access requests registered by CDAWeb for *Wind* and OMNI data (which largely relies upon *Wind* and ACE measurements) between Jan. 1, 2015 and Jan. 1, 2017. Because of its longevity, *Wind* observations will allow researchers to compare long-term variations in solar wind properties, solar wind transients, and micron-sized dust fluxes for solar cycles 22–24 without needing to compensate for changing instrumentation and calibration. Furthermore, new *Wind* data, produced since the last Senior Review, will **provide unprecedentedly accurate and high time, energy, and angular resolution measurements of the near-Earth solar wind.**

*Wind* continues to remain a relevant mission as evidenced by recent press releases and high impact publications (i.e., **12 in *Nature* and 7 in *Phys. Rev. Lett.*** since 2015), for instance at:

http://www.nature.com/articles/srep08080;
https://www.nasa.gov/feature/goddard/2016/nasa-finds-unusual-origins-of-high-energy-electrons.

*Wind* has also contributed critically to multi-mission studies, as part of the Heliophysics System Observatory (HSO). With its ample fuel reserves, sufficient for >50 years, *Wind* will continue to provide accurate solar wind input for magnetospheric studies (supporting MMS, THEMIS, and *Van Allen Probes*) and serve as the 1 AU reference point for outer heliospheric (e.g., *Voyager*, MAVEN, JUNO) investigations, in addition to providing critical support for other NASA missions (e.g., STEREO, ACE, DSCOVR, etc.). Moreover, new *Wind* results will continue to improve theories of solar wind heating, acceleration, and energetic particle processes to focus the science objectives of future missions (e.g., *Solar Probe Plus* and *Solar Orbiter*). Once these new missions are launched, ***Wind* will provide critical measurements to complement the observations made by *Solar Probe Plus* and *Solar Orbiter* which will enable researchers to relate the solar wind at 1 AU to its coronal sourse and compare radio burst power with source locations.**

### Rationale for Continuing the *Wind* Mission

- *Wind* continues to provide unique, robust, and high resolution solar wind measurements
- *Wind* will serve as the 1 AU reference for *Solar Probe Plus* and *Solar Orbiter*
- *Wind* aids in cross-calibration efforts for the DSCOVR and ACE missions
- *Wind* and ACE are complementary not identical ⇒ both are needed for complete 1 AU observations
- *Wind* still has redundant systems, instruments, and enough fuel for >50 years
- *Wind*'s high scientific productivity → significant discoveries in all three SMD research objectives

# Table of Contents

# 1 Science and Implementation

## 1.1 Historical Background

The *Wind* spacecraft was launched in November, 1994 as the interplanetary component of the Global Geospace Science (GGS) Program within ISTP. *Wind*'s original purpose was (1) to make accurate in-situ measurements of interplanetary conditions upstream of the magnetosphere to complement measurements made in the magnetosphere by *Polar* and *Geotail* and (2) to remotely sense interplanetary disturbances for possible future predictive purposes. The instruments were therefore designed to make highly accurate solar wind measurements.

Prior to May 2004, *Wind* performed a series of orbital maneuvers (see Figure 2) that led to: ∼67 petal orbits through the magnetosphere; out of the ecliptic plane lunar rolls in April and May of 1999; four east-west prograde 1:3–Lissajous orbits reaching $\gtrsim$300 $R_E$ along the ±Y-GSE direction between August 2000 and June 2002; and an excursion to the L2 Lagrange point from November 2003 to February 2004 (i.e., >220 $R_E$ downstream of Earth and ∼500 $R_E$ downstream of ACE). In May 2004, *Wind* moved to L1 where it has remained and will stay for the foreseeable future. Note that *Wind*'s L1 orbit has a ±Y-GSE displacement about the sun-Earth line of ∼100 $R_E$, much larger than ACE or DSCOVR.

## 1.2 Current Status

The *Wind* spacecraft continues to operate in good health. In 2000, the team successfully reconfigured the communications system to enhance the telemetry margin. Reliance on a single digital tape recorder (with two tape units, TUA and TUB) since 1997 has never hampered operations, and the team took measures to minimize its use in order to extend tape recorder life as long as possible.

Seven of the eight *Wind* instruments, including all of the particles and fields instruments, remain largely or fully operational. The EPACT, high energy particle, and SMS solar wind composition instruments suffered some degradation, but both continue to provide valuable measurements. The SWE electron instrument required some reconfiguration to maintain its capabilities. The TGRS $\gamma$-ray detector was been turned off, as planned due to it no longer having sufficient coolant to operate. For technical details see Section 5.2.

In May 2014 the 3DP instrument (specifically PESA Low) suffered an anomaly that only affected the telemetry house keeping data. The science data remained unaffected and continues to return the highest resolution velocity moments of the solar wind of any near-Earth spacecraft. All the other instruments operate nominally. Thus, the net loss in capability remains minimal and the *Wind* instruments continue to provide definitive and continuous measurements of the solar wind.

On Oct. 27, 2014 at 21:59:38 GMT, the *Wind* command and attitude processor (CAP) suffered two single event upsets (SEUs). The redundant nature of the *Wind* spacecraft bus allowed the flight operations team (FOT) to successfully switch to a second CAP, CAP2. The FOT began the recovery of CAP1 on Jan. 21, 2015 and finished Jan. 30, 2015. Thus, the *Wind* spacecraft was fully recovered at ∼17:50 UTC on Jan. 30, 2015. For more details, please see Section 5.1.

On April 11, 2016 one of the two tape units (TUA) began experiencing issues related to the read/write head causing ∼few percent data loss per day. The flight operations team successfully switched the primary record unit to TUB on May 6, 2016 to extend the life of TUA and reduce data loss. *Wind* continues to average >98% data recovery rates and the TUB status is fully operational.

In conclusion, *Wind* is operationally healthy and continues to maintain a large fuel reserve, capable of sustaining the spacecraft at L1 for >50 years.

## 1.3 *Wind*'s Unique Capabilities

*Wind*'s complement of instruments was optimized for studies of solar wind plasma, interplanetary magnetic field, radio and plasma waves, and of low energy particles. The instrument suite is not equivalent to that of ACE; rather the two missions complement each other. ACE – launched ∼3 years after *Wind* – focuses on the detailed investigation of high energy particles for which *Wind* has more limited capabilities. Several of *Wind*'s solar wind, suprathermal particle, and especially radio and plasma wave instruments are unique. *Wind*'s instrument capabilities are summarized in Table 1 and are compared to ACE and STEREO. ***Wind* is unparalleled for low energy particle and radio wave observations of the solar wind by near-Earth spacecraft.** A more detailed discussion of *Wind*'s unique capabilities follows below.

Collaborating with STEREO, *Wind*/WAVES provides an essential third vantage point along the Sun-Earth line, allowing the unambiguous localization of inner heliospheric radio sources and the determination of their corresponding beam patterns. More importantly, *Wind* is the only spacecraft at L1 that can observe the upper hybrid line (or plasma line), which provides the most accurate and only unambiguous measurement of the total electron density in the solar wind. Thus, the density – normally obtained as a moment or fit of the velocity distribution

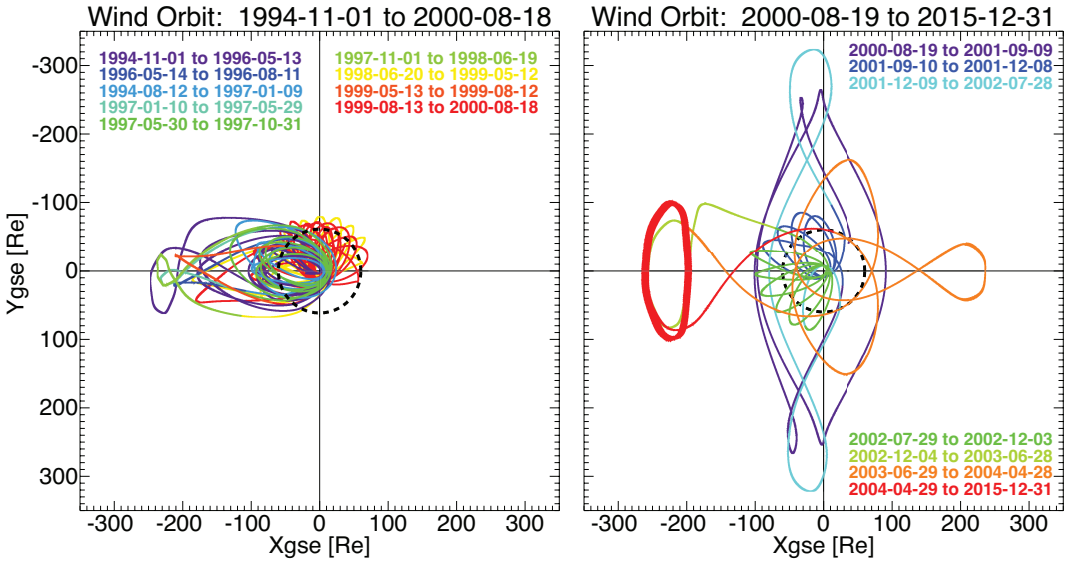


**Figure 2:** *Orbital trajectories of the Wind spacecraft in the GSE XY plane from 1 November 1994 to 31 December 2015. Colors denote time ranges as indicated. The dashed black circle indicates the Moon's orbit (Adapted from Figure 1 in Malaspina and Wilson III [2016]).*

function from particle instruments like SWE and 3DP – can be accurately and independently derived from the WAVES instrument. **The WAVES instrument provides the only method for an independent, in-flight, and absolute calibration for particle instruments for spacecraft near L1.**

*Wind* is unparalleled in its capacity for high time resolution (HTR) measurements of quasi-static magnetic fields (MFI instrument) and thermal solar wind electrons (3DP). Though STEREO/SWEA has a higher cadence in burst mode, the low energy ($\lesssim$60 eV) electrons cannot be measured by the detector [e.g., *Fedorov et al.*, 2011], causing *Wind*/3DP to have the highest time resolution measurements of thermal electrons. *Wind*/MFI offers continuous coverage of the quasi-static magnetic fields at ∼11 samples per second (sps) over the entire mission (∼22 sps when *Wind* was within $\lesssim$100 $R_E$ of Earth), still the highest sample rate of science-quality, continuous solar wind measurements.

*Wind*/STICS is unique among currently operational spacecraft as it is the only sensor in space fully dedicated to providing measurements of heavy ions for an energy range spanning ∼6.2–223.1 keV/amu. As STICS is a time-of-flight mass spectrometer, it can differentiate many minor ionic species and look at their characteristics in the suprathermal energy range to better understand their origin. In addition, *Wind*/LEMT provides high energy particle data over a range of energies not covered by ACE (i.e., ∼1–10 MeV/amu).

The *Wind*/WAVES instrument can also be used for solar energetic particle (SEP) studies. For instance, *Malandraki et al.* [2012] and *Agueda et al.* [2014] made detailed comparisons of the injection time histories of selected SEP events, as derived from the modeling of the interplanetary transport of electrons and protons, with electromagnetic emissions, particularly with decametric-hectometric (DH) type III radio bursts. A close correspondence was found, and this underlines the usefulness of type III bursts as a constraint of energetic particle release to interplanetary space. *Wind* is still the only near-Earth spacecraft which can measure both the electromagnetic and particle signatures of SEP events. **Thus, *Wind*'s distinct capacities make it as a valuable asset to the Heliophysics community and an essential component in the HSO.**

## 1.4 Heliophysics System Observatory

*Wind* plays an active role in the Heliophysics System Observatory (HSO). *Wind* achieved many of its recent scientific discoveries in collaboration with other spacecraft as described in more detail in Section 4. Participation in the HSO enables more such collaborative studies in the future, by providing a data environment where such comparisons can be readily performed. As the Heliophysics Data Policy outlines, this data environment requires the presence of in-depth metadata for each data product based on a uniform standard (the SPASE dictionary). It also envisions the eventual connection of the distributed data repositories by a number of virtual observatories enabling the location and downloading of the desired data. *Wind* plays a leadership role in the deployment of the Virtual Heliospheric Observatory (VHO), the heliospheric portion of this environment, and the gen-

**Table 1:** The measurement capabilities of *Wind* compared to STEREO and ACE

| Type | *Wind* | STEREO | ACE | Comments for *Wind* |
|---|---|---|---|---|
| DC Magnetic Field | MFI ~11 sps[a] | MAG ~8 sps, (~32 sps burst) | MAG ~6 sps | highest time resolution for continuous coverage |
| Radio Waves | WAVES ~4kHz–14MHz | S/WAVES ~2.5kHz–16MHz | N/A | unique large antenna length allows for measurement of local plasma frequency → electron density |
| Time Domain Waveforms | TDS ~1.9–120ksps[b] | TDS ~7.8–250ksps | N/A | search coil and long antenna → better calibration and more sensitive |
| Thermal Ions (Moments) | 3DP[c] SWE ~92 s | PLASTIC ~60 s | SWEPAM ~64 s | highest time, angular, and energy resolution; robust and redundant; operates during solar storms |
| Thermal Ions (DFs[d]) | 3DP ~24 s[e] | PLASTIC N/A | SWEPAM N/A | highest time, angular, and energy resolution |
| Thermal Electrons (Moments) | 3DP (~3 s) SWE (~9 s) | SWEA[f] (~2 s) | SWEPAM (~128 s) | highest time resolution for full $4\pi$ coverage at low energy |
| Thermal Electrons (DFs) | 3DP ~3 s | SWEA ~2 s | SWEPAM N/A | [same as above] |
| Solar Wind Composition | SMS/STICS 1≤Z≤56 ~0.3–230keV/Q | PLASTIC 1≤Z≤56 ~0.3–80keV/Q | SWICS 1≤Z≤30 ~0.5–100keV/Q | only observations > 100 keV/Q |
| Mass Spectrometry | SMS/MASS 1≤Z≤28 ~0.5–12keV/Q | N/A N/A N/A | SWIMS 2≤Z≤30 ~0.5–20keV/Q | comparable to ACE in both charge and energy |
| Low Energy Electrons | 3DP ~3eV–500keV | SWEA[g] SEPT[h] STE[i] | SWEPAM EPAM ~3eV–400keV | full 3D measurements from a few eV to ~500 keV |
| Low Energy Ions | 3DP ~3eV–7MeV | SEPT ~60keV–7MeV | SWEPAM[j] EPAM[k] ULEIS[l] | measurements of solar wind thermal core to lower energies |
| High Energy Particles | EPACT/LEMT ~0.04–50MeV/n | SIT[m] LET[n] HET[o] | SIS CRIS ~10–600MeV/n | robust; high geometry factor; unique directional observations; and energy range |

[a] ~22 samples per second when inside 100 $R_E$; [b] kilosamples per second;
[c] moments: ~3s, distributions: ~24s, burst: ~3s; [d] DF = velocity distribution function; [e] ~3s in burst mode;
[f] nothing below ~60eV; [g] ~60–3000eV; [h] ~2–100keV, 4/8 telescopes contaminated; [i] ~30–400keV;
[j] ~260eV–35keV; [k] ~46–4800keV; [l] ~45keV/n–2MeV/n; [m] ~0.03–5MeV/n; [n] ~2–60MeV/n; [o] ~1–170MeV/n;

eration of the corresponding metadata.

The Living With a Star (LWS) program seeks to better understand the Sun-Earth connected system with the aim of developing reliable space weather forecasting capabilities. The program architecture plan calls for a near-Earth solar wind monitor to connect the solar (SDO) and inner heliospheric (e.g., *Solar Probe Plus* and *Solar Orbiter*) observations with geomagnetic ones (e.g., *Van Allen Probes*). **However, NASA has no plans for a new solar wind and solar energetic particle (SEP) monitoring mission until at least 2024.** Rather NASA assumes that *Wind*, ACE or both will survive into the 2017–2022 time frame. DSCOVR has only limited measurement capabilities (Faraday Cup and magnetometer) and fuel only for about five years, leaving *Wind* and ACE still as the primary near-Earth assets during the primary phase of the *Solar Probe Plus* and *Solar Orbiter* missions. The lowest risk option to satisfy the near-Earth solar wind monitoring re-

quirement of LWS is to sustain both *Wind* and ACE – either of which can satisfy the LWS measurement requirements – because both are well past their prime missions and design lifetimes. Again, note that *Wind* and ACE are not duplicate spacecraft but rather serve complementary roles. Thus, the most prudent course of action involves preserving both spacecraft.

In the following we discuss our progress on the previous set of Prioritized Science Goals (PSGs).

## 2 Previous PSGs

**Prior Prioritized Science Goals**

1. Long-term variations: Two Full Solar Cycles
2. Solar Wind Structures
3. Kinetic Signatures of Heating and Acceleration
4. Dust science

The *Wind* mission is operating on a minimal budget that does not allow for the dedicated support of any in-depth focused scientific research. The funding is applied to the operation of the spacecraft and the collection and validation of high quality solar wind measurements. As part of the instrument data validation process, several significant scientific discoveries have been made in recent years as outlined in the following sections. Most detailed scientific research using *Wind* data is primarily supported under the ROSES GI and SR&T programs. In the following sections, we outline several *Wind* results relating to our past focused science research topics.

### 2.1 PSG #1: Two Full Solar Cycles

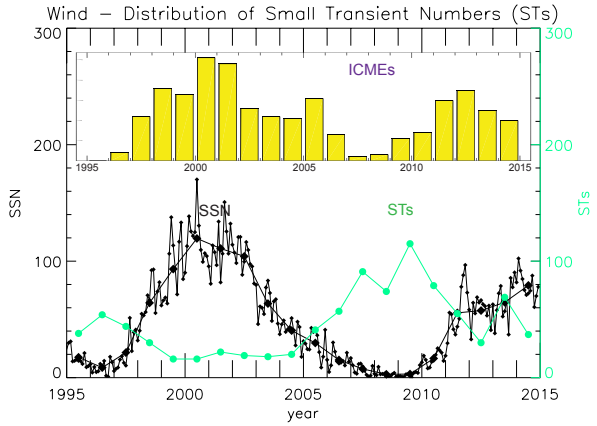


**Figure 3:** *Distribution of yearly numbers of STs observed by Wind (green trace) from 1995–2014. The sunspot numbers (SSN) are shown in black. The top panel gives a histogram of ICMEs (yellow) from published tabulations [e.g., Richardson and Cane, 2010] (Adapted from Figure 11 in Yu et al. [2016]).*

*Wind* was launched at the tail end of solar cycle (SC) 22 (i.e., March 1986 to May 1996) and has provided continuous measurements through all of SC23 (i.e., June 1996 to December 2008) and the current extent of SC24 (i.e., January 2009 to Present) [*Hathaway*, 2015] in its >22 years of operation. Thus, *Wind* has at least some solar wind data from three different solar cycles. The time range included for this Senior Review will likely cover the rest of SC24 and may include the beginning of SC25. In this section we discuss some recent progress towards understanding the dependence of long-term phenomena on the solar cycle.

One of the many phenomena thought to be dependent upon the SC are solar transients, e.g., coronal mass ejections or CMEs. Small transients (STs) – magnetic field configurations whose passage at Earth may last from a few tens of minutes to a few hours – have gained recent interest due to their relationship with the slow solar wind. *Yu et al.* [2016] presented a statistical study of STs observed by *Wind* and STEREO for the 20 year period 1995–2014 (STEREO only from 2006 onward).

**Table 2:** ICME Parameters over 3 Solar Cycles (Adapted from *Nieves-Chinchilla et al.* [2017])

| **Parameter** | **SC22[a]** | **SC23** | **SC24** |
|---|---|---|---|
| # of Events | 13 | 169 | 119 |
| # of Days[b] | ∼577 | ∼4597 | ∼2556[c] |
| # of Events/Year[d] | ∼8 | ∼13 | ∼17 |
| $\langle B \rangle$[e] [nT] | N/A | ∼12 | ∼10 |
| $\langle V_{sw} \rangle$[f] [km/s] | N/A | ∼459 | ∼381 |
| $\langle n_p \rangle$[g] [cm$^{-3}$] | N/A | ∼7.3 | ∼7.7 |
| **Parameter** | **Min[i]** | **Max[j]** | **Mean[k]** |
| $\lvert B \rvert$ [nT] | ∼3 | ∼33 | ∼11 |
| $\lvert V_{sw} \rvert$ [km/s] | ∼270 | ∼968 | ∼433 |

[a] SC = solar cycle; [b] # of Julian days of *Wind* coverage; [c] up to Dec. 31, 2015 or ∼7730 total days; [d] 365 day years; [e] average over SC coverage; [f] solar wind bulk flow speed; [g] proton number density; [h] minimum of all events; [i] maximum of all events; [j] average of all events;

Figure 3 presents the long-term (including data from three SCs) occurrence frequency of STs vs. the SSN (black line) and ICMEs (yellow histogram). A clear anti-correlation with SSN is evident. The ST number peaks in 2009, a year of a deep solar minimum. This trend is opposite to that of large ICMEs. Similar results were obtained by the STEREO probes far from the Sun-Earth line. The plot raises several questions in light of the recent "weak" SC.

In addition to STs, another phenomenon whose study benefits greatly from three SCs of data is ICMEs. ICMEs are manifestations of magnetized plasma moving from the Sun throughout the helio-

sphere and also main triggers of geomagnetic activity. These solar transient structures are often characterized by a well organized magnetic structure embedded within the ICME, known as Magnetic Clouds (MCs). Developing a reliable space weather forecasting system requires the simultaneous observation of the velocity, size, plasma density, and magnetic topology of ICMEs.

*Nieves-Chinchilla et al.* [2017] performed a statistical study of ICMEs observed by *Wind* from 1995–2015. Table 2 summarizes some of the SC properties of magnetic obstacles from the *Wind* ICME catalogue (https://wind.gsfc.nasa.gov/ICMEindex.php).

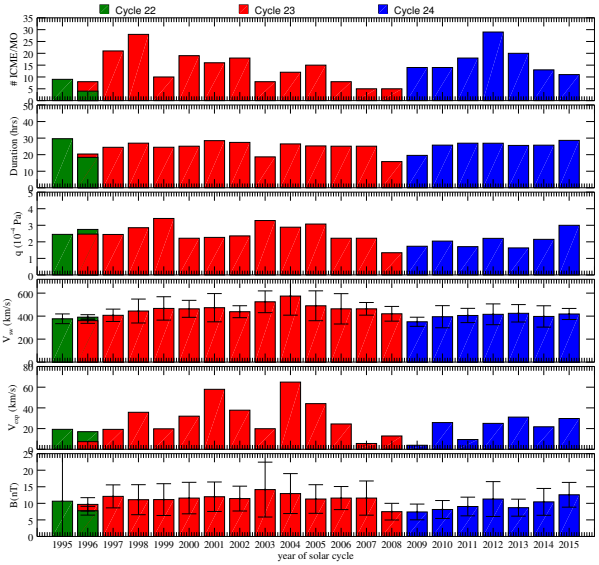


**Figure 4:** *Summary of ICME statistics by year of the SC from the Wind ICME catalogue for SC22 (green), SC23 (red), and SC24 (blue). The panels shown are yearly averages of the following (in order from top-to-bottom): # of ICMEs with embedded flux-ropes; flux-rope duration [hrs]; dynamic pressure [Pa]; solar wind bulk flow speed [km/s]; flux-rope expansion speed [km/s]; and magnetic field magnitude (Adapted from Nieves-Chinchilla et al. [2017]).*

Figure 4 compares the yearly averages of ICMEs from the *Wind* ICME catalogue for SC23 (red) and SC24 (blue). The expansion speed is defined as one-half the difference between solar wind bulk speed at the start and end time of the flux-rope embedded within the ICME. The maximum number of ICMEs appears earlier in SC23 than SC24, which exhibits a "bell shaped" profile with a maximum in year 4 (i.e., 2012). The average yearly rate of events is 14 for both SC23 and SC24 (e.g., see Table 2). The dynamic pressure resembles a bimodal distribution for SC23 but is less well pronounced for SC24. The solar wind speed and magnetic field magnitudes, however, show little solar cycle dependence. However, for both parameters SC24 shows slightly weaker values than SC23.

These studies highlight the SC dependence of solar wind transient structures. *Wind*-related work has also found that SEPs and solar flares depend upon the SC [*Dierckxsens et al.*, 2015]. Further, the presence of continuous coverage can improve the accuracy of long-term predictive models of solar cycles [e.g., *Zachilas and Gkana*, 2015]. These studies provide illustrative examples of **the importance of continuous coverage by a single spacecraft over long durations, like *Wind*, without which such investigations would suffer.**

## 2.2 PSG #2: Solar Wind Structures

Small transients (STs) – magnetic field configurations whose passage at Earth may last from a few tens of minutes to a few hours – may play a role in the development of the slow solar wind. As mentioned in the previous section, an extensive statistical study of the occurrence and properties of small solar wind transients (STs) was presented by *Yu et al.* [2016]. It was based on *Wind* and STEREO data for the 20 year period 1995–2014. The authors examined the dependence of ST occurrence frequency in (i) solar cycle phase, and (ii) solar wind speed during the STs. They define the latter by taking the average speed of the STs since these transients tend to convect with the surrounding flow.

Figure 5 shows the distribution of solar wind speeds for STs as observed by *Wind* and both STEREO spacecraft. The huge majority of STs lie in the slow wind. The velocity distribution peaks in the ∼300–400 km/s velocity bin for all three spacecraft. This velocity dependence is much stronger than that of the solar cycle. For example, we contrast the ST occurrence in 2009 with that of 2003. Roughly 27% of 2003 corresponded to slow solar wind while ∼89% of 2009 was slow solar wind (i.e., ∼3.3 times higher). Rather than observing ∼3 times as many STs in 2009 as in 2003, the authors reported ∼6.4 times as many. Thus, the authors argue that the STs may be an important constituent of the slow solar wind.

The *Wind* mission has been providing in situ plasma, energetic particles, and magnetic field observations since late 1994. The *Wind* team maintains an online catalogue (https://wind.gsfc.nasa.gov/ICMEindex.php) of Earth-directed ICME events with well organized magnetic topology – known as Magnetic Clouds (MCs) – observed by *Wind* from 1995–2015. MCs are defined here as the interval within an ICME where the magnetic pressure dominates over the plasma pressure (i.e., sub-unity plasma $\beta$) with an organized magnetic topology similar to the conceptual picture

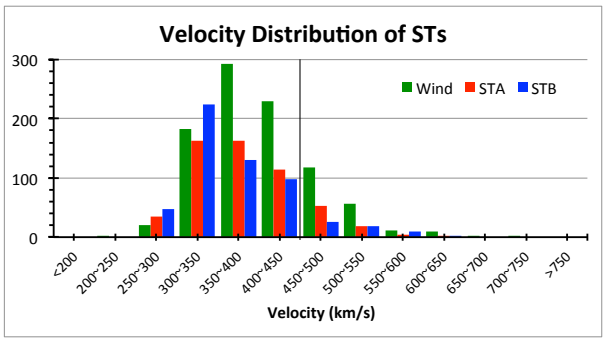


**Figure 5:** *Velocity distribution of STs as measured by Wind from 1995–2014 and both STEREO spacecraft from 2006–2014. A vertical line has been drawn at $V \sim 450$ km/s, separating slow from fast winds (Adapted from Figure 12 in Yu et al. [2016]).*

of a heliospheric flux-rope (FR). The main webpage of the ICME catalogue presents links to the years included in the catalogue.

The following are included for each event: ICME start and end times; magnetic obstacle start and end times; a link to the associated interplanetary (IP) shock (i.e., at http://www.cfa.harvard.edu/shocks/wi_data/) if present; the magnetic obstacle classification; mean magnetic field; solar wind bulk velocity; and the expansion velocity [*Nieves-Chinchilla et al.*, 2017]. The magnetic obstacle, embedded within the ICME, is defined as a FR – traditionally called magnetic clouds or MCs – for events with at least one magnetic rotation and ejecta (E) when no clear magnetic topology is detected. Every event also includes a link to a plot of the data for the event and a link to the integrated Space Weather Analysis system (iSWA, https://iswa.gsfc.nasa.gov/), which presents an overview of the state of the heliosphere during the ICME propagation to the Earth.

Figure 6 shows an example ICME observed by *Wind* on January 1, 2010. The EEP parameter (i.e., last panel) was introduced by *Nieves-Chinchilla et al.* [2016] to quantify the bi-directionally of the electrons. The EPP is the ratio of the average electron intensity of the parallel (i.e., 0°–18°) and anti-parallel (i.e., 162°–180°) pitch-angles to the perpendicular (i.e., 78°–96°) pitch-angles. The inner-two dashed lines (i.e., from 2010-01-02/00:24:00 UT to 2010-01-03/08:38:00 UT) enclose the flux-rope (i.e., MC) defined by an increase in magnetic field magnitude, rotation in $B_z$, and low $\beta_p$. The first dashed line (i.e., at 2010-01-01/22:04:00 UT) shows the start of an IP shock followed by the sheath region. It can be seen that the EPP goes to zero at the IP shock and remains there until roughly the second half of the flux-rope. The bi-directional electron flows during the second half suggest a connection of both ends

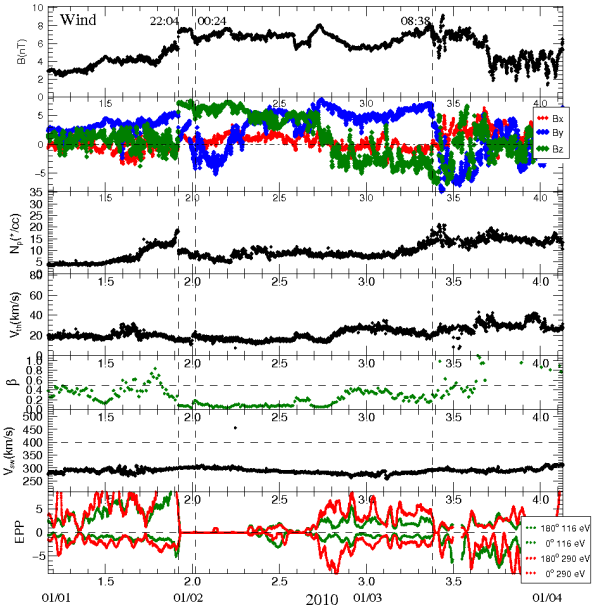


**Figure 6:** *In situ data from the MFI and SWE instruments onboard the Wind spacecraft on January 1, 2010. The panels shown are the following (in order from top-to-bottom): magnetic field magnitude; magnetic field components (GSE); proton number density; proton thermal speed; proton beta, $\beta_p$; solar bulk flow speed; and the Electron Pitch-angle distribution (PAD) Parameter (EPP), for 116 and 290 eV electrons. The vertical lines show the interval of the ICME front and flux-rope boundaries (Adapted from Figure 5 in Nieves-Chinchilla et al. [2016]).*

of the field line to the sun.

Our current understanding of the magnetic field topology, structure, global morphology, and the effect of the evolution of ICMEs is still limited. The >22 years of continuous *Wind* observations provide an opportunity to examine the effects of the ICME expansion, distortion, or interaction with ambient solar wind. To study the effect ICME expansion on their evolution, *Nieves-Chinchilla et al.* [2017] defined a Distortion Parameter (DiP) – the amount of asymmetry of the magnetic field strength – and compared it to the ICME expansion speed ($V_{exp}$).

Figure 7 (top) shows the range of DiPs vs. $V_{exp}$. Regions with $V_{exp}$ <(>) 0 correspond to a contracting(expanding) ICME. The DiP parameter range is from 0.0–1.0. A DiP $< 0.5$ implies a magnetic field compression occurs closer to the spacecraft's first encounter with the ICME (i.e., ICME start time). A DiP $> 0.5$ implies the magnetic field compression occurs closer to the ICME end time. One would expect to have more compression closer to the ICME start time (i.e., decreasing DiP $< 0.5$) as $V_{exp}$ increases for expanding ICMEs. An examination of Figure 7 shows that the events do not follow the expected relation-

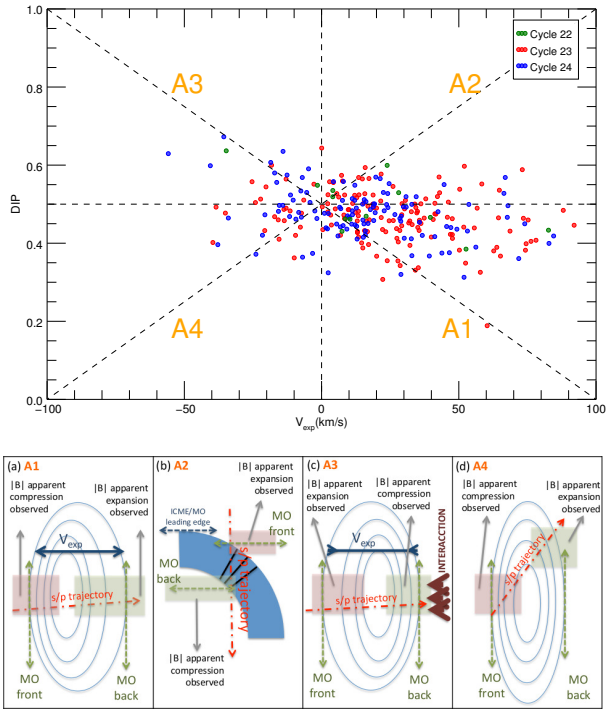


**Figure 7:** ***Top:*** *Distortion Parameter (DiP) is shown versus the flux-rope expansion velocity ($V_{exp}$). The $V_{exp}$ interval goes from -100 km/s to 100 km/s. The negative value of the expansion velocity represent the compression. DiP interval goes from 0 to 1, with symmetry profile at DiP = 0.5, magnetic field strength compression in the front with DiP < 0.5 and magnetic field compression in the back with DIP > 0.5.* ***Bottom:*** *Schematic cartoon illustrating the differences in flux-rope shape/trajectory for the four quadrants labeled in the top figure (Adapted from Nieves-Chinchilla et al. [2017]).*

ship between the $V_{exp}$ and DiP. Instead, one finds an homogeneous spread.

Figure 7 (bottom) provides a cartoon representation of the possible magnetic field configurations associated with each quadrant in Figure 7 (top). A visual analysis of individual quadrants (i.e., A1, A2, A3, A4) suggests that the discrepancy could be affected by expansion (A1) or also by distortion (A4), curvature (A2), or interaction with the solar wind or other transients (A3). Thus, the preliminary results suggest all effects may play a role in causing the difference between the expected and observed results.

*Wind*'s large database of STs and ICMEs has provided us with a large enough number of events to perform significant statistical studies on both the general properties and SC dependence. *Wind*-related work has given us evidence that ICMEs exhibit evidence of distortion, curvature, and effects due to interaction with the solar wind or other transients. **It is only because of large statistics due to the long-term, continuous coverage of *Wind* that researchers have been able to examine and begin to understand the evolution of the solar wind transients responsible for the most dramatic geoaffective space weather events.**

## 2.3 PSG #3: Kinetic Physics

In the following section, we highlight new results of kinetic signatures of heating and acceleration using *Wind*. As will be clear from the length of this section compared to the other prior PSGs, *Wind*'s unique instrument suites allow for a broad range of kinetic studies.

One of the major goals of *Wind* EPACT-LEMT was to extend measurements of element abundances in solar energetic particle (SEP) events throughout the periodic table. LEMT resolves individual elements up to $Z = 26$ ($Fe$), and groups similar similar-$Z$ elements together for higher $Z$ up to $Z = 82$ ($Pb$). However, in small impulsive events these observations have revealed a strong power-law enhancement, relative to coronal abundances, that rises by a factor of ~1000 from $He$ to $Pb$, as a function of the mass-to-charge ratio, $A/Q$, as seen in Figure 8.

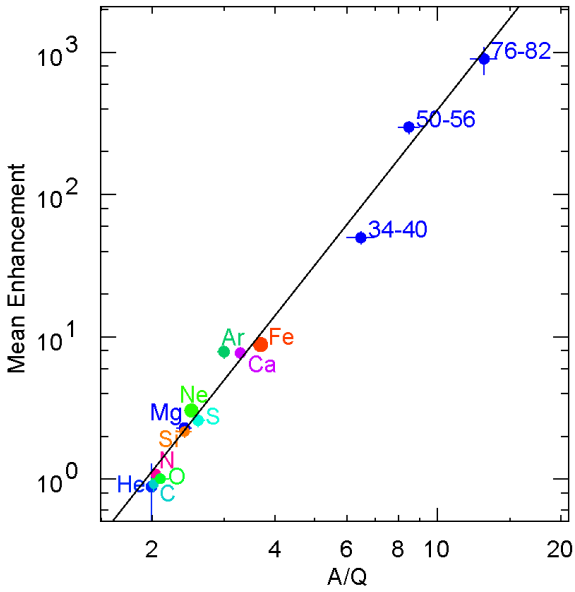


**Figure 8:** *The mean element enhancement in impulsive SEP events (relative to coronal abundances) is shown vs. $A/Q$ at 2.5–3.2 MK where values are taken from the shaded band in Figure 9. The power of the fitted line shown is 3.64 ± 0.15 (Adapted from Figure 14 in Reames [2015]).*

The pattern of abundances in Figure 8 is driven by ionization states $Q$ that only occur at the plasma temperatures found in solar active regions. For example, in solar active regions $C$ is fully ionized like $He$, and thus un-enhanced, while the enhancement of $Ne$ exceeds that of $Mg$ and $Si$, etc. Individual impulsive

SEP events are strongly bound to this thermal region [*Reames et al.*, 2015]. These enhancements are believed to result from islands of magnetic reconnection [e.g., *Reames*, 2016a,b,c, and references therein] that occur in solar jets, reconnecting with open magnetic-field lines where ions easily escape. A similar process in flares leads mainly to heating since the accelerated ions are trapped on closed loops.

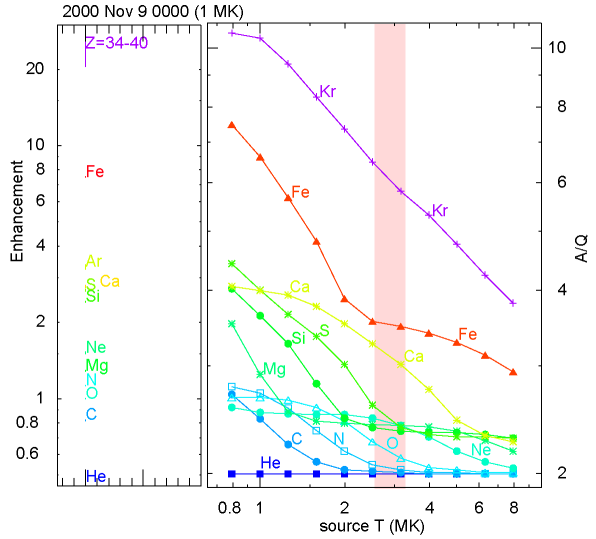


**Figure 9:** *The left panel shows enhancements in element abundances seen during the large gradual event of 2000 November 9. The right panel shows $A/Q$ vs. $T$ for various elements. The shaded region shows solar active-region temperatures. The groupings of enhancements match those in $A/Q$ near 1 MK (Adapted from Figure 3 in Reames [2016a]) (Reames 2016a, b, c).*

It has been known for many years that power-law enhancements can also occur in large gradual SEP events involving acceleration at CME-driven shock waves. Here, either enhancements or suppressions can result from $A/Q$-dependent scattering during transport, often both occur in a single event. *Reames* [2016a] and *Reames* [2016b] found that these power-law dependences can also be used to measure source plasma temperatures as shown in Figure 9. Here observed enhancements in an event, on the left, are compared with the theoretical values of $A/Q$ vs. $T$ on the right. For this event, the best fit can be shown to occur at a temperature near 1 MK, an ambient coronal temperature. Note that here $C$, $N$, and $O$ are enhanced, more like $Ne$ than $He$, and $Si$ and $S$ have moved up near $Ar$ and $Ca$. This pattern is quite unlike that found for the higher-temperature active region shown as shaded.

In a study of 45 large gradual events [*Reames*, 2016a], ~70% had source plasma temperatures of the ambient corona (<1.6 MK) while ~25% had active-region temperatures (2.5–3.2 MK). This implies that in ~25% of the events, the shock waves sweep across active regions and re-accelerated some residual suprathermal ions from earlier enhanced impulsive SEP events, diluted by some of the local plasma.

Source temperature variations explain many of the subtle event-to-event abundance variations, and comparisons of impulsive and gradual events at similar temperatures suggest that the shocks are averaging over many small impulsive events that must take place almost continuously in active regions [*Reames*, 2016b]. In the process, a new way to measure ionization states at the point of acceleration was derived, unmodified by traversal of material afterward; this is especially important for impulsive SEP events that occur fairly low in the corona. **These new *Wind* results are finally helping us to understand the physics of the energetic particle enhancements originally observed over 30 years ago.**

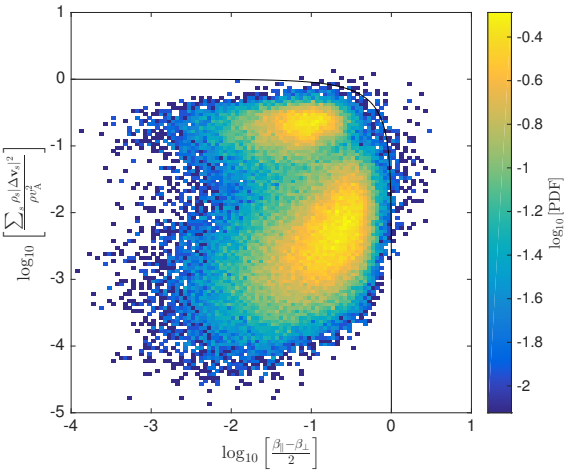


**Figure 10:** *2D histogram of solar wind parameters relevant to the firehose instability. The x-axis represents the total pressure anisotropy of all species, and the y-axis represents the drifts between all species. The black line marks the long-wavelength firehose threshold, with the data constrained to the stable side. Two populations can be seen, corresponding to the presence or absence of proton beams. Adapted from Figure 2 in Chen et al. [2016].*

In recent years, *Wind* has revealed to us the role played by various plasma instabilities in controlling the bulk solar wind parameters. In particular, the firehose and mirror instabilities have been shown to constrain the plasma beta and temperature anisotropy of each particle species. *Chen et al.* [2016] combined the newly calibrated *Wind*/3DP electron data set and the newly fitted *Wind*/SWE ion data set (with proton beams) to examine these instabilities in a full multi-species context for the first time.

Using the theoretical long-wavelength firehose condition, it was found that the anisotropy and drifts

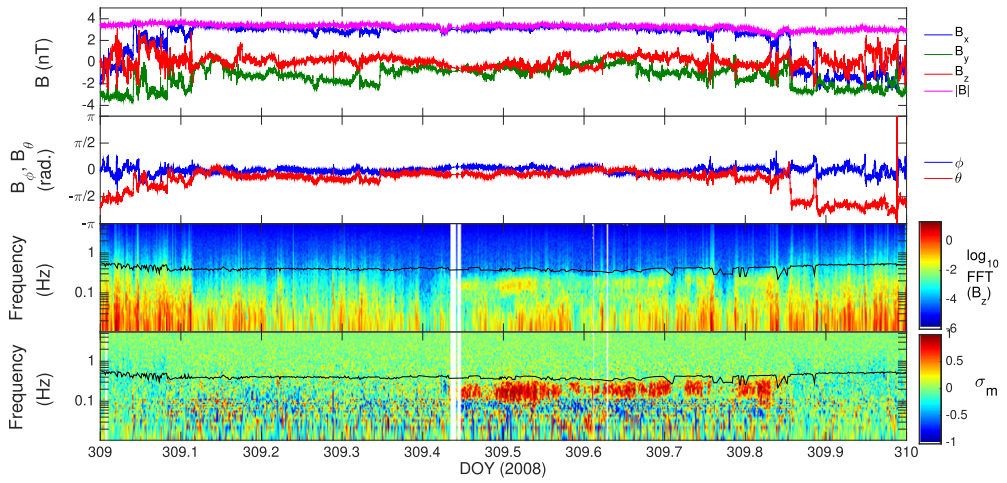


**Figure 11:** *Example date with long-duration ion cyclotron waves (ICWs) simultaneously observed with a drifting proton beam by Wind. The panels shown are the following (in order from top-to-bottom): magnetic field magnitude (magenta) and GSE components; magnetic field latitude (blue) and longitude (red); $B_z$ dynamic power spectrum; and reduced magnetic helicity. The black line across the bottom two panels is the proton gyrofrequency Doppler-shifted into the spacecraft frame (Adapted from Figure 1 in Wicks et al. [2016]).*

of all major particle populations (proton core, proton beam, electrons, alphas) contribute to the instability, with protons dominating the anisotropy, and drifts contributing more than half in the presence of a proton beam (see Figure 10). Using the theoretical long-wavelength mirror condition, protons were also found to dominate this instability, but with non-proton species contributing more than one third. Overall, this multi-species examination of these instabilities, enabled by the high-quality instrumentation and large data set of *Wind*, showed that the combined thresholds work well in constraining the solar wind parameters. These results are important for understanding how the instabilities operate, and how they constrain plasma evolution, both in the solar wind, and in other astrophysical environments where direct measurements are not possible.

Another recent study found a more direct relationship between the in situ particle velocity distributions and electromagnetic wave activity. *Wicks et al.* [2016] examined a long-duration ion cyclotron wave (ICW) storm observed simultaneously with a secondary drifting proton beam (i.e., drifting relative to the core solar wind protons). Figure 11 shows data from the interval of the ICW storm.

Using linear Vlasov theory, the group found that the observed proton distributions were unstable to a temperature anisotropy instability (i.e., $T_\perp > T_\parallel$) of both the core and proton beam. During some intervals only the core or beam satisfied $T_\perp > T_\parallel$ but during the intervals with the most intense wave activity, both satisfied this constraint. The authors also found that the wave and beam kinetic energy densities were positively correlated.

Similar instability studies were carried out by *Gary et al.* [2016] and *Jian et al.* [2016]. Using the well-calibrated (core and beam) proton and alpha particle data from *Wind*-SWE and the high-cadence magnetic field data from *Wind*-MFI, they studied the left-hand polarized Alfvén-cyclotron instability driven by an ion temperature anisotropy and the right-hand polarized magnetosonic instability driven primarily by relative flows between different ion components. The study by *Jian et al.* [2016] was carried out during periods of fast solar wind and that of *Gary et al.* [2016] during slow solar wind. They found some of the enhanced magnetic field fluctuations were consistent with the radiation of ICWs – characterized by left-hand circular polarization, parallel/anti-parallel (with respect to $\mathbf{B}_o$) propagation, and frequency near the proton cyclotron frequency – from the Alfvén-cyclotron instability. In a minority of events, the observed wave modes were consistent with magnetosonic waves – characterized by right-hand circular polarization, parallel/anti-parallel propagation, and frequencies extending well beyond the proton cyclotron frequency – radiated by the magnetosonic instability. The non-thermal ion velocity distribution features were found to be the source of free energy for both instabilities.

The solar wind electron velocity distribution function exhibits a variety of features that deviate from thermal equilibrium. These deviations from equilibrium provide a local source for electromagnetic fluctuation emissions, including the commonly observed electron whistler-cyclotron and firehose instabilities. *Adrian et al.* [2016] presents a systematic analysis of *Wind*-SWE-VEIS observations of solar wind electron

plasma and associated *Wind*-MFI observed magnetic fluctuations.

Figure 12 presents a statistical overview of the *Wind*-SWE-VEIS observations of the solar wind electron distribution occurrence frequency and normalized magnetic fluctuation amplitudes sorted by fast ($V_{sw} \geq 500$ km/s) and slow ($V_{sw} < 500$ km/s) solar wind speed. The data are plotted against theoretical thresholds for parallel propagating electron cyclotron-whistler instability (black lines for $\gamma = 10^{-1}\ \Omega_{ce}$, $\gamma = 10^{-3}$ and $10^{-4}\ \Omega_{ce}$), obliquely propagating electron whistler-mirror mode instability for $\theta = 40°$ (dark gray dashed line for $\gamma = 10^{-3}\ \Omega_{ce}$) and the parallel electron firehose instability (light gray dashed lines for $10^{-4}\ \Omega_{ce}$) that have been derived by *Viñas et al.* [2015] assuming both bi-Maxwellian (M) and Tsallis kappa-like ($\kappa$) electron distributions. The location of the maximum occurrence pixel of each distribution has been indicated using an open-Maltese cross. The bottom row of Figure 12 presents the distribution of normalized magnetic fluctuation amplitudes ($\delta B/B_o$) as a function collisional age ($A_E$) for slow (left) and fast (right) solar wind. Note that the distribution of normalized fluctuation amplitudes for slow solar wind remains relatively flat with respect collisional age with a centroid located at $\sim 7.0 \times 10^{-3}$. The distribution for fast solar wind is quite distinct with its collisional age limited to values below 60 and possessing a broadened/elongated distribution of amplitudes centered at a collisional age of $A_E \sim 6$.

For the first time, *Adrian et al.* [2016] exploit the full solar wind electron distribution function and its moments, without separation of the various electron components (i.e., core, halo, and strahl) and find evidence that the temperature anisotropy threshold of the parallel electron cyclotron anisotropy instability (or parallel whistler anisotropy instability) bounds solar wind electrons during slow solar wind periods. Further, these authors demonstrate that during periods of slow solar wind, collisions, while infrequent, are the dominant mechanism by which solar wind electrons are constrained, leading to isotropization. During fast solar wind periods, magnetic fluctuations and solar wind anisotropies are enhanced above the parallel whistler anisotropic threshold boundary and collisional effects are significantly reduced. Preliminary calculations presented by *Adrian et al.* [2016] show that the oblique electron whistler mirror anisotropic instability bounds both the slow and fast solar wind. Regardless of speed, the solar wind electron thermal anisotropy appears globally bounded by the parallel electron firehose instability for anisotropies $T_{e\perp}/T_{e\parallel} < 1$. The results of *Adrian et al.* [2016] indicate that collisions, while infrequent, play a necessary role in regulating the solar wind electron velocity distributions. In striking contrast to solar wind ions, solar wind electron plasma, when considered globally as a single electron velocity distribution function, is only marginally stable with respect to parallel propagating instabilities.

While the work presented by *Adrian et al.* [2016] makes it tempting to establish analogies between their results for electrons and those of protons reported by *Bale et al.* [2009], one must remember that the thermal properties of electrons are very different from those of ions; including their characteristic times and spatial scales for wave-particle interactions. Furthermore, the collisional processes that control the electrons and protons occur on very different scales, as clearly demonstrated by the results of *Adrian et al.* [2016].

The conclusions presented by *Adrian et al.* [2016] must also be taken with some level of caution. While the volume of solar wind electron data considered by *Adrian et al.* [2016] is comparable to that presented by *Bale et al.* [2009] for solar wind protons, the electron data considered by *Adrian et al.* [2016] only encompass ∼5% of a solar cycle in contrast to that of *Bale et al.* [2009]. As such, solar cycle phase effects cannot be addressed through the analysis presented by *Adrian et al.* [2016] and there is evidence in the SWE-VEIS data from the first *Wind* orbital element identified that suggests – but not presented in their manuscript – that an organization of the data as a function of Carrington rotation exists. Future studies are underway to incorporate additional viable, independent SWE-VEIS electron plasma observations from the remaining fifty-three *Wind* orbital segments identified by *Adrian et al.* [2016] into the results presented in their original work. In addition, these authors have launched efforts to separate the SWE-VEIS solar wind electron plasma observations into their basic constituents – core, halo and strahl – and in an effort to repeat their analysis for each component separately, thereby systematically replicating the efforts of *Štverák et al.* [2008], but in far greater detail.

It is important to note that the three studies by *Chen et al.* [2016], *Wicks et al.* [2016], and *Adrian et al.* [2016] were only possible because of the massive number of observations accumulated by the *Wind* spacecraft. For instance, the separation of the proton core and beam is a newer data product that required large statistics to distinguish a secondary proton beam from the more typical drifting alpha-particle population.

While many studies in recent years rely upon *Wind* only as a solar wind monitor, it is important to rec-

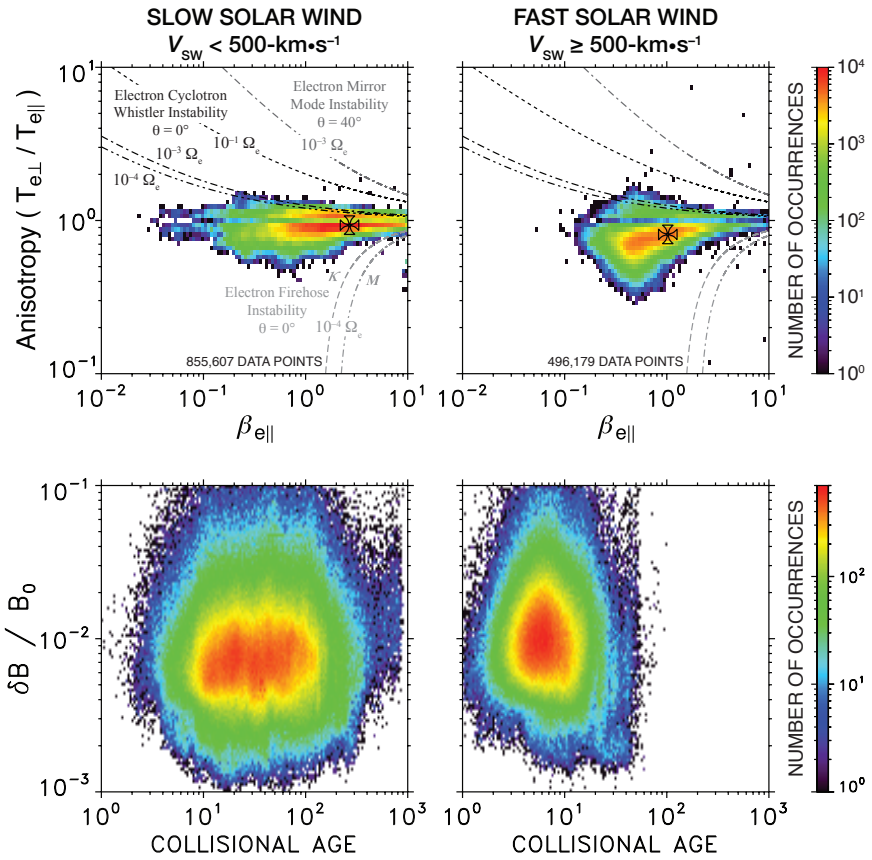


**Figure 12:** *A statistical overview of the Wind SWE-VEIS observations of the solar wind electron distribution occurrence frequency organized as a function of parallel electron beta ($\beta_{e\parallel}$) and electron temperature anisotropy ($T_{e\perp}/T_{e\parallel}$) in the top row and the normalized magnetic fluctuations ($\delta B/B_o$) as a function collisional age ($A_E$) in the bottom row, for slow solar wind speed ($V_{sw}$ < 500 km/s, left column) and fast solar wind ($V_{sw} \geq$ 500 km/s, right column). Over plotted in the top row are labeled instability thresholds discussed in the text. (Adapted from Figures 3 and 9 in Adrian et al. [2016]).*

ognize that despite its 22+ year age *Wind* continues to produce new and exciting results. **These studies illustrate the importance of *Wind* as a high quality, stand-alone space plasma laboratory because it is the only spacecraft continuously in the solar wind capable of making such measurements.**

## 2.4 PSG #4: Dust Science

It was only recently that researchers realized that a certain type of impulsive, "spikey" waveform signal observed the *Wind*/WAVES time domain sampler (TDS) receiver was the product of hypervelocity dust impacts. It was later determined that the signals corresponded to micron-sized (i.e., dust grains approximately ∼1 $\mu$m in size) interplanetary dust (IPD) and interstellar dust (ISD) [e.g., *Malaspina et al.*, 2014]. The relevance of dust to the heliospheric community has increased in recent years with the recognition that it plays an important role in numerous ways from mass, momentum, and energy transport to physical damage to spacecraft (e.g., cutting of wire antenna).

There are two potential mechanisms proposed to explain the impulsive electric field signatures observed by waveform capture instruments: (1) the spacecraft body changes electric potential after the impact but the antenna do not; and (2) the charge cloud produced by the impact interacts with the antenna directly. It was only recently determined that both mechanisms are at play on *Wind* [*Kellogg et al.*, 2016]. This was determined by comparing the dust flux rate early in the mission to that later in the mission. The reason is that one side of the ∼100 m tip-to-tip wire antenna (x-antenna) was cut (it is assumed by dust) twice, once on August 3, 2000 and the second time on September 24, 2002. Thus, prior to the first cut the x-antenna responded as an electric dipole and was insensitive to changes in the spacecraft potential. During this period, the number of impacts was lower by factors ∼1.5–3.0 compared to periods after the cut. Therefore, it appears likely that the

second mechanism may contribute more to the total number of dust impacts than the first.

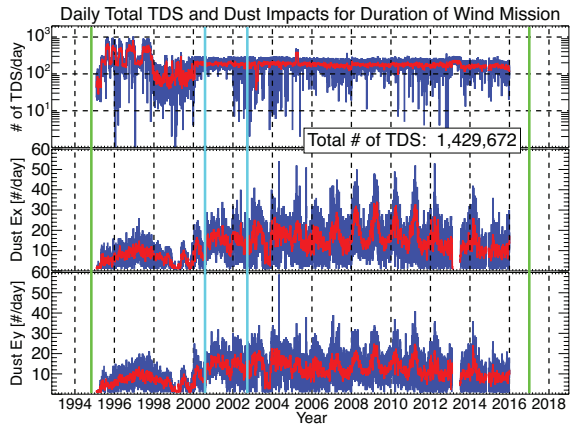


**Figure 13:** *Plot of the entire Wind mission showing the daily totals. In each panel the dark blue and red lines represent the actual and 10-day smoothed counts, respectively. The panels shown are the following (in order from top-to-bottom): total number of TDS events per day; number of dust impacts observed on the x-antenna; and number of dust impacts observed on the y-antenna. The two vertical green lines define the current duration of the Wind mission. The two vertical cyan lines define the times when the x-antenna was cut (Adapted from Figures 5 and 6 in Malaspina and Wilson III [2016]).*

Figure 13 shows the counting statistics for TDS events and dust impacts observed by the *Wind* TDS receiver. The obvious annual variation in dust impacts seen in the bottom two panels is primarily due to ISD. The reason is that for half of the year, *Wind* is moving approximately anti-parallel to the flow of ISD through the solar system. The difference in flow speed of the ISD in *Wind*'s reference frame varies from ∼4–56 km/s, thus leading to an annual variation in the counting rates (i.e., higher impact speeds produces larger electric field amplitudes and thus more dust observations). This annual variation has been reported in multiple studies [e.g., *Kellogg et al.*, 2016; *Malaspina and Wilson III*, 2016; *Malaspina et al.*, 2014; *Wood et al.*, 2015].

*Wind* is a south-ecliptic spin-stabilized spacecraft. This allowed *Malaspina et al.* [2014] to estimate a the direction from which the incident dust must have arrived. Both *Malaspina et al.* [2014] and *Wood et al.* [2015] found that their estimates of the ISD impact direction were consistent with the expected interstellar flow direction. Thus, the annual variation in dust impacts is entirely due to ISD as IPD has no preferred direction in the solar rest frame. With the large number of impacts recorded by *Wind* due to its longevity and relatively large impact target area (i.e., the spacecraft bus), it was also determined that *Wind* does not respond to nanodust (i.e., grains with $\ll$0.1 $\mu$m in size) [e.g., *Kellogg et al.*, 2016; *Malaspina and Wilson III*, 2016; *Malaspina et al.*, 2014].

These results illustrate *Wind*'s unique capabilities and the importance of its longevity. For instance, ***Wind* independently verified the direction of ISD flow showing it agrees with predictions and results from *Ulysses*; a critical piece of information for current and future heliospheric and astrophysical missions. These results have improved our understanding of the interaction between the heliosphere and the local interstellar medium.**

## 2.5 Noteworthy Studies

Unfortunately, there is not sufficient room to explain in detail all the new and exciting work performed since the last Senior Review. However, we thought it necessary to mention several works that were not explicitly discussed in our PSG progress reports from the previous sections. Some of the work below derived from *Wind*'s unique complement of instruments (e.g., the KONUS gamma-ray detector) while others were outside the scope of our prior PSGs. Regardless we thought it necessary to at least briefly mention these studies in the short list shown below.

1. Highlight on ultra-long-duration gamma ray bursts: [*Greiner et al.*, 2015]
2. Discovery of electron acceleration to relativistic energies in ion foreshock: [*Wilson III et al.*, 2016]
3. Highlight on solar wind reconnection: [*Xu et al.*, 2015]
4. Shock acceleration of electrons during large SEP events: [*Tan and Reames*, 2016]
5. Shock acceleration of heavy ions: [*Gruesbeck et al.*, 2015; *Nitta et al.*, 2015; *Wang et al.*, 2016]
6. Relationship between solar radio bursts and ICMEs: [*Salas-Matamoros and Klein*, 2015; *Suresh and Shanmugaraju*, 2015; *Vasanth et al.*, 2015]
7. SEP, solar flare, and ICME dependence upon SC: [*Dierckxsens et al.*, 2015]
8. Electron superhalo observations during quiet solar wind periods: [*Wang et al.*, 2015]

# 3 New Prioritized Science Goals

| New Prioritized Science Goals |
|---|
| 1. Wave- and/or Turbulence-Particle Studies |
| 2. Unusual Solar Cycle |
| 3. Particle Acceleration |
| 4. Long-Term Dust Science |

Again, we emphasize that the *Wind* mission is operating on a minimal budget that does not allow for

the dedicated support of any in-depth focused scientific research (e.g., see Section 6). In the following sections, we outline a number of prioritized and focused science research topics that the *Wind* instrument teams are planning to undertake during the next five years as per the proposal call.

## 3.1 Field-Particle Studies

*Wind* still retains some of the highest resolution measurements of near-Earth spacecraft and is the only L1 spacecraft capable of measuring both DC- and AC-coupled electric and magnetic fields. These unique measurements make *Wind* a unique observatory for examining the kinetic physics involved in the interaction of particles with fluctuating electromagnetic fields, whether coherent wave modes or turbulence. In this section we introduce some novel ideas for future *Wind* investigations combining measurements of both electromagnetic fields and particle velocity distributions.

### 3.1.1 Turbulence Studies

*Wind* shares a instrument suite similar to that of Solar Probe Plus (SPP), which will allow for comparative analysis of measurements from each set of instruments. For instance, during periods of nearly radial conjunction, tests of the evolution of turbulence and particle velocity distributions will be possible. Of particular interest will be cross-comparison studies between *Wind* and other missions like ACE, DSCOVR, SPP and Solar Orbiter (SolO) to examine the large-scale dynamics of solar wind turbulence. Constraints provided by long intervals of these system-scale multipoint observations will enable comparisons with global solar wind simulations driven by magnetograms and corona observations [*Lionello et al.*, 2014; *Usmanov et al.*, 2014]. Long baseline correlations of electron observations from inner heliospheric observations (SPP) and *Wind* electrons will enable studies of magnetic field line topology and wandering. These studies will be able to quantify the effects of turbulence over 1 AU scales, a crucial element for estimating error in Space Weather prediction.

*Wind* also plays an important role in a recently implemented [*Matthaeus et al.*, 2016] method for understanding the intrinsic time dependence of solar wind magnetic field turbulence. This method also enables direct examination of the accuracy of the Taylor hypothesis (i.e., the frozen-in flow approximation) that allows researchers to convert temporal observations into spatial correlation. After accumulating numerous datasets, this method provides the full space-time correlation (in the plasma frame). Although not precise for any individual data interval, for a suitable defined ensemble, such as slow wind or fast wind, the method permits study of the breakdown of the Taylor hypothesis at various scales. This approach employs many pairs of multi-spacecraft observational intervals, and becomes more useful and accurate as the ensemble becomes better populated. This study provides a useful database that can help interpret the single spacecraft datasets obtains by Solar Probe Plus and Solar Orbiter. As this fundamental dataset is accumulated and improved it can provide predictions for effects of time decorrelations that will be observed during near-radial alignments of the constellation of heliospheric spacecraft, including *Wind*.

The partition of energy between electrons, protons, and minor ion species is a major issue in understanding the acceleration and extended heating of the solar wind and the heating of the corona. *Wind*'s unique set of thermal plasma measurements provide an invaluable testbed for the very active theoretical and simulation work on this fundamental subject. For example, the ratio $T_e/T_p$ provides constraints for both turbulence and kinetic plasma theory. Further, *Wind*'s newly calibrated electron data, combined with $T_p$ and $\mathbf{B}_o$, can be used to further pin down heating rates due to turbulence and relate them to theory [e.g., *Matthaeus et al.*, 2016]. The same approach using large datasets may be used to test theoretical developments that aim to predict how the heating rates and partition of energy between electron and protons can be related to inertial and dissipation range properties. A common thread in these developments is that stronger turbulence should produce more significant coherent structures at ion scales. This can lead to greater distortions in the particle distributions, fueling additional kinetic processes eventually leading to heating and/or acceleration. Our current understanding suggests that coherent structures tend to increase the intermittency and local heating in the plasma. Local heating at proton scales appears to be correlated with steeper sub-proton scale spectra as well as large magnetic fluctuation amplitudes at the proton gyroscale. **Turbulence remains an active and important topic in understanding the structure and dynamics of the heliosphere, and *Wind* data has been central in many of the basic studies that have been done and that are planned to be done, particularly in the new SPP and SolO era.**

### 3.1.2 Wave/Instability Studies

Given the recent increased interest in kinetic scale phenomena, *Wind*'s importance to the community has only increased. *Wind*'s 22+ year age will allow researchers to perform both case studies [e.g., *Wicks et al.*, 2016] and long-term statis-

tical studies [e.g., *Adrian et al.*, 2016; *Chen et al.*, 2016] of wave/instability interactions with particles. The results from past studies have already helped to improve the science definitions for future missions like SPP and SolO. Further, many of the wave/instability-particle studies using *Wind* are used as critical tests and constraining criteria for the development of new missions like the Interstellar MApping Probe (IMAP) and Turbulence Heating ObserveR (THOR).

With the release of the entire electron distribution function moments (i.e., account for spacecraft potential) and the future release of the velocity moments of the electron components (i.e., core, halo, and strahl), tests of wave/instability-particle interactions will be more readily available. We expect these new higher level data products to improve the science return of *Wind* and future missions. Further, the necessary enhancements in time resolution for missions like SPP and SolO arose by necessity because the time scales for the same phenomena at 1 AU decrease with decreasing distance from the sun. The time resolution of many of *Wind*'s instruments are comparable to SPP and SolO when normalized to physical parameters (e.g., local cyclotron frequency). **Thus, *Wind* will continue to play a critical role in the study of kinetic physics resulting from wave/instability interactions with particles.**

### 3.1.3 New Analysis Techniques

As the community becomes increasingly aware of the relevance of kinetic-scale processes to the evolution of the solar wind and other macroscopic phenomena (e.g., collisionless shocks), the need for the continued operation of *Wind* becomes more obvious. The instrument teams continue to improve the calibration and accuracy of the measurements each year because the increasing number of data points reduces the statistical uncertainties in many parameter calculations. Below we highlight a specific new analysis technique that will be employed in wave- and/or turbulence-particle studies over the coming years.

Typically, the analysis of particle velocity distribution functions requires a strong, technical understanding of the instrument and calibration schemes. Thus, these steps have traditionally been carried out by the instrument teams using semi-automated analysis software. The automated routines are optimized for typical solar wind conditions, so they can fail to capture the complex (and scientifically interesting) microphysics of transients in the solar wind (e.g., CMEs), which are often better analyzed manually.

The recently released, publicly available (https://github.com/JanusWind/FC) *Janus* software (created by Bennett Maruca, funded under NASA Awards NNX15AF52G and NNX17AC72G) is now providing the scientific community with a new paradigm for analyzing thermal ion measurements from *Wind* and other spacecraft. *Janus* provides users with an easy-to-use graphical user interface (GUI) for carrying out highly customized analyses of ion velocity distributions without need for detailed background information or prior knowledge of the instrument idiosyncrasies. This will allow users from the entire community to examine the thermal ion velocity distributions in detail for the first time.

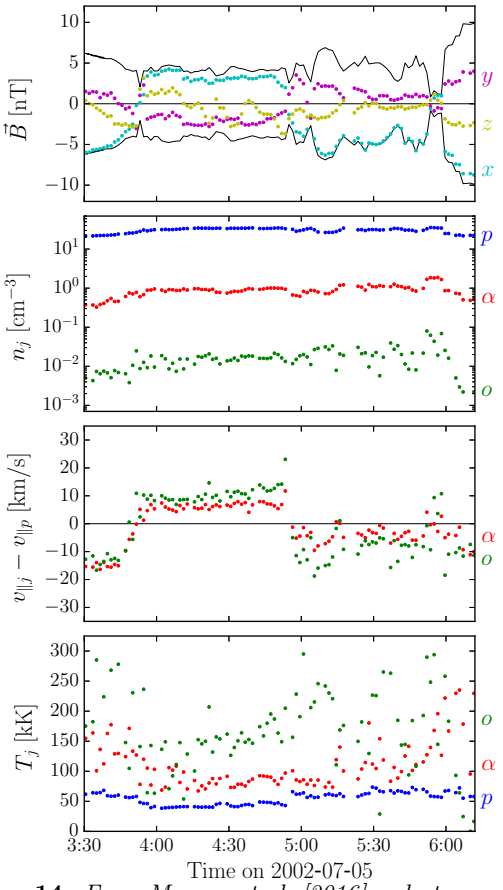


**Figure 14:** *From Maruca et al. [2016], select parameters from the* Janus *analysis of an exemplar period of FC measurements of the solar wind. From top to bottom, these plots show the magnetic field (from Wind/MFI), ion density, ion differential flow (relative to protons), and ion temperature. For protons and α-particles, the plotted values are of "total" parameters, which incorporate both the beam and core populations.*

Version 1 of *Janus*, released late last year [*Maruca et al.*, 2016], focuses specifically on measurements from the *Wind*/SWE Faraday Cups (FC). Though the moments and reduced distribution functions from the SWE-FCs has been publicly available on CDAWeb, *Janus* allows the user to perform their own analysis on the thermal ion velocity distributions.

Figure 14 presents an example output from *Janus* of FC measurements from a particularly dense ($n_p \approx 30$ cm$^{-3}$) period of slow ($V_p \approx 350$ km/s) solar wind. The high density allowed the FCs to resolve a third species, $O^{6+}$, in addition to the usual protons and alpha-particles. Both the protons and alpha-particles exhibited distinct core and halo components, giving a total of three species and five populations analyzed. The density trends for these three species were very similar, suggesting a steady relative abundance. Further, the drift between the protons and both the alpha-particles and $O^{6+}$ were very similar, though the latter tended to be slightly faster. The ion temperatures were consistently ordered by particle mass (with $O^{6+}$ usually hottest), but the relationship was less than mass proportional (possibly due to collisional thermalization) [*Kasper et al.*, 2008; *Maruca et al.*, 2013].

Two extensions of *Janus* are now under development. First, the team is adapting *Janus* to analyze the 3DP thermal ion measurements from the two electrostatic analyzers (ESAs) called PESA Low and High. The two PESA instruments can resolve a full 3D velocity distribution from a few 10s of eV to ~30 keV, which will allow users to explore the ion velocity distribution functions for evidence of non-Maxwellian features (e.g., kappa and skew-normal distributions).

Second, *Janus* will be expanded so that it can jointly process measurements from the FCs and PESA Low. This will be the first time that data from FCs and ESAs have been combined. It will draw upon the strengths of each detector to produce higher quality solar wind ion parameters. Furthermore, this will serve as an important case study for SPP [*Fox et al.*, 2016], which will also have both a FC and an ESA for measuring thermal ions. However, unlike their counterparts on *Wind*, the SPP instrument fields-of-view will only slightly overlap. For instance, SSP is frequently expected to encounter periods during which the combined FC and ESA measurements will provide nearly complete coverage of the thermal ions but will not individually [e.g., see Figure 9 in *Kasper et al.*, 2016]. **Therefore, the adaptation of the *Janus* software to perform such a joint analysis is especially important and will benefit both the *Wind* and SPP missions.**

## 3.2 Unusual Solar Cycle

As of November 1, 2016 *Wind* marked 22 years of continuous operation only surpassed in age (for currently operational spacecraft) by SOHO, *Geotail*, and the two *Voyagers*. Long-term solar cycle investigations, whether they are about large-scale structures or solar wind conditions, critically depend on continuous high quality observations. These studies can be severely hindered when multiple spacecraft are used due to the complexities and time consuming efforts of instrument inter-calibration. Therefore, the continuation of *Wind* becomes even more beneficial to the community.

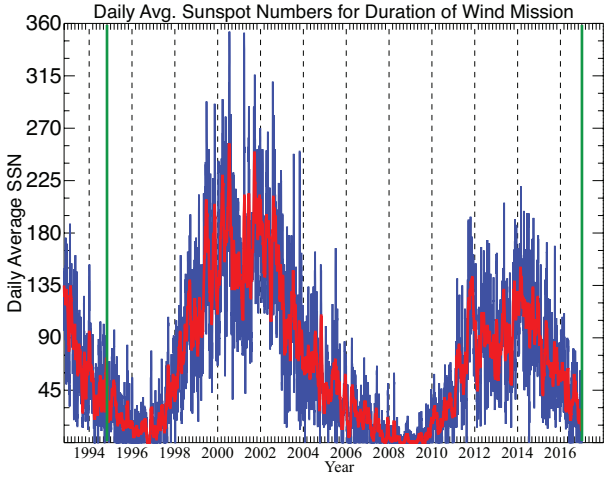


**Figure 15:** *Daily (blue line) and 27 day smoothed (red line) average sunspot numbers (SSNs) for the duration of the Wind mission (defined by vertical green lines). The data are taken from http://www.sidc.be/silso/infosndtot.*

As was previously illustrated, *Wind*'s continuous, long-term observations have resulted in several lists of SC-dependent phenomena like ICMEs [e.g., *Nieves-Chinchilla et al.*, 2017] and interplanetary shocks (e.g., http://www.cfa.harvard.edu/shocks/wi_data/). The next SC's effect on these phenomena is obviously not known but continuation of *Wind* through FY22 should provide statistics into SC25. The additional information will help the community improve predictive capabilities for space weather and long-term phenomena.

As we enter an "unusual" solar minimum following an "unusual" solar maximum, it is important to maintain continuous coverage of the solar wind. The weaker than normal solar maximum of SC24 is evidenced in Figure 15. It is also important to remember that this solar minimum/maximum will share the same magnetic polarity as SC22, allowing for direct comparison with the early *Wind* measurements of cosmic rays and elemental abundances [e.g., *Reames*, 1999]. The magnetic polarity was also found to affect the 27 day variations associated with solar rotation [e.g., *Reames and Ng*, 2001], an effect which must be confirmed with new observations in the impending solar minimum.

Regardless of the predictions, the operation of *Wind* through FY22 would provide the community with a continuous array of datasets that span from the end of SC22 to the beginning of SC25, all near-

Earth measurements. Given that the observed and predicted trends in solar behavior suggest we are entering a long-term solar minimum [e.g., *Zachilas and Gkana*, 2015], the importance of maintaining a single, uniform dataset is further magnified. **Thus, the rationale for continuing the *Wind* mission through FY22 becomes obvious.**

### 3.3 Particle Acceleration

Upstream of a magnetized collisionless shock there can be a region in communication with the shock – the foreshock – unlike collisionally mediated shocks like in Earth's neutral atmosphere. Foreshocks occur upstream of quasi-parallel magnetized shocks, where the shock normal angle ($\theta_{Bn}$) between the upstream quasi-static magnetic field ($\mathbf{B}_o$) and the shock normal vector satisfies $\theta_{Bn} < 45°$. Foreshocks are primarily populated by suprathermal ions reflected/energized by the shock and streaming against the incident bulk flow. The relative drift between the incident and reflected ions can drive numerous instabilities [e.g., *Wilson III*, 2016], some of which are wave-like and others are structure-like. For brevity, let us refer to the structure-like transient phenomena as *foreshock disturbances* – large-scale (∼1000 km to >30,000 km), solitary (∼5–10 per day), transient (lasting ∼10s of seconds to several minutes) structures [e.g., *Omidi and Sibeck*, 2007; *Turner et al.*, 2013; *Wilson III et al.*, 2016] that are generated by the free energy in the streaming between reflected suprathermal (>100 eV to 100s of keV) and incident solar wind ions [e.g., *Burgess et al.*, 2012; *Wilson III*, 2016].

The recent discovery that foreshock disturbances can locally generate relativistic electrons up to ∼300 keV [e.g., *Wilson III et al.*, 2016] has raised several questions about our understanding of shock acceleration. Some of these structures had been found to locally generate field-aligned ion beams [e.g., *Wilson III et al.*, 2013] and even their own miniature foreshocks [e.g., *Liu et al.*, 2016]. Prior to these studies, it was not thought possible for these structures to efficiently accelerate electrons let alone generate energies an order of magnitude higher than thought possible at the bow shock. Subsequent investigation of many more foreshock bubbles has found electrons with energies in excess of ∼700 keV [*Personal communication with Terry Z. Liu, Dec. 13, 2016*].

The suprathermal ion pool between ∼2–10 times the solar wind speed provides most of the seed population for corotating interaction region (CIR) and CME-associated shocks in the inner heliosphere. *Wind*'s SMS/STICS, EPACT/STEP, and EPACT/LEMT provide unique measurements of the composition and energy spectra of suprathermal ions through energies between ∼3 keV/e - 20 MeV/nucleon. Thus, *Wind* provides near-complete spectral and compositional coverage of the suprathermal seed populations as well as the accelerated populations during large gradual SEPs, $^3$He-rich impulsive SEPs, and recurrent particle events associated with CIRs. Using STEP data, *Filwett et al.* [2017] recently showed that the ∼20-320 keV/nucleon heavy ion population in 41 CIRs observed from 1995–2008 most likely originates from the re-acceleration of a ∼20–80 keV/nucleon suprathermal population that was measured upstream a few days earlier. Further, they found that this suprathermal population is accelerated within ∼1 AU of Earth-orbit. These results are at odds with the traditional model in which CIR particles observed at 1 AU are accelerated at shocks between ∼3–5 AU and then transported to Earth-orbit, but are instead consistent with the more recent *Wind* observations [e.g., *Ebert et al.*, 2012a,b].

The solar minimum of SC25 offers an unprecedented opportunity to combine *Wind*, ACE, and STEREO observations with those from SPP and SolO to track the evolution of compression regions from inside ∼0.2 AU and determine where they start accelerating particles. In addition, the *Wind* team will combine observations of Type II and Type III radio bursts with in-situ suprathermal and SEP data with remote sensing data from STEREO and SDO to identify and study the properties of a variety of solar source regions of SEP events (e.g., flares, jets, filaments, coronal shocks etc.). During the latter portion of the senior review period, we will use SolO and SPP to track the evolution of transients, CMEs, and their shocks and make significant progress on separating the effects of acceleration and transport that routinely blur the interpretation of SEP events observed near Earth-orbit.

The unique capabilities of the 3DP SST instrument to measure the full angular dependence of protons in the energy range from ∼100 keV up to a few MeV allows researchers to test the predictions of classical diffusive shock acceleration (DSA) for near-isotropic intensities against advanced models, which take into account the pitch-angle and gyrophase dependence as well as focused transport and adiabatic deceleration the solar wind/magnetic field structures in the inner heliosphere [e.g., *Gedalin et al.*, 2016; *Kartavykh et al.*, 2016]. The above effects can be expected to lead to measurable differences in the spectrum of the accelerated particles as a function of the the shock angle and the compression ratio, and could provide further insight about the energization of particles at astrophysical shocks.

**These studies have altered our understanding of shock acceleration and have raised ques-**

**tions about local vs. remote pre-energization (i.e., the so called "injection problem"). Thus, we will exploit the newly processed *Wind* datasets from SMS, EPACT, and 3DP to look for evidence of local vs. remote shock acceleration and continue to aid with and advance foreshock and bow shock studies.**

### 3.4 Long-Term Dust Science

David M. Malaspina (PI) and Lynn B. Wilson III (Co-I) created a dust impact database [*Malaspina and Wilson III*, 2016] for the entire *Wind* mission (currently from Jan. 1, 1995 to Dec. 31, 2015). The database can be found at CDAWeb (https://cdaweb.gsfc.nasa.gov). The *Wind* database is the only ∼21 year long record of micron (i.e., dust grains approximately ∼1 $\mu$m in size) interplanetary dust (IPD) and interstellar dust (ISD) at 1 AU with currently >107,000 impacts. The authors intend to update the database from its current state (1) in early 2017 to extend it through 2016, (2) when the final *Wind*/TDS data is sent to SPDF/CDAWeb, and (3) once every two years for the continuing duration of the mission.

The publicly available database now allows researchers to perform long-term investigations of the phenomena (e.g., ICMEs) that may influence ∼1 $\mu$m dust grains. The database also overlaps by 12 years with the *Ulysses* dust database allowing for cross-comparison. The primary advantage of the *Wind* database is that the entire spacecraft body acts as the collecting area (i.e., $\gtrsim$4.3 m$^2$ excluding top/bottom decks) in contrast to missions with dedicated dust detectors, where the effective collecting area is ∼0.1 m$^2$ (e.g., *Ulysses*' dust instrument [e.g., *Gruen et al.*, 1992]). Consequently, *Wind* has recorded >107,000 impacts. This is over an order of magnitude more impacts than *Ulysses* (∼6700) over its 16 year mission life [e.g., *Wood et al.*, 2015] and Cassini's ∼36 ISD impacts over ∼10 years of data [e.g., *Altobelli et al.*, 2016]. While the *Wind* database does not define the impactor's speed, mass, or composition, the large number of impacts is unique and absolutely critical for statistical studies and long-term investigations.

Finally, the database is not only useful for the heliophysics and planetary communities, it is important for mission planning (e.g., SPP and SolO) and the astrophysics community. The importance and unique value of this dataset will only increase as we enter an historically unusual period of solar activity. Further, the planned launch of SPP and SolO is in 2018, which is during the second half of this proposal period. **Therefore, *Wind* can serve as a "standard candle" for dust observations to which both SPP and SolO can compare.**

## 4 *Wind* in the HSO

As part of the Heliophysics System Observatory (HSO), *Wind* has been contributing to numerous science investigations that rely on multi-spacecraft observations. Many of these have been described in the preceding sections. In addition, *Wind* observations are also critical to many other spacecraft, enabling and enhancing their mission success. This is evidenced by the **over 600 refereed publications and the >1,825,000 data access requests on CDAWeb since the last Senior Review.** This section outlines some of these functions *Wind* serves.

### 4.1 Inner Heliospheric Missions

#### ACE

*Wind* and ACE have been working under mutual calibration support for several years in order to increase the scientific value of each mission. *Wind*'s capacity to measure the total electron density using the WAVES radio receivers to observe the upper hybrid line (or plasma line) is unique among every L1 spacecraft and most near-Earth spacecraft (*Van Allen Probes* and MMS have this capacity as well). This unambiguous measurement of the total electron density coupled with two independent thermal ion plasma measurements (3DP and SWE) give *Wind* three separate measurements for cross-calibration resulting in highly accurate thermal plasma observations. Further, the SWE instrument can operate even during intense high energy particle events associated with solar flares and CMEs. The robustness of *Wind*'s instrumentation and measurements makes it a invaluable asset for near-Earth solar wind monitoring and other spacecraft. For instance, the ACE SWEPAM team uses *Wind*'s thermal plasma observations to help improve their calibrations. We expect to continue this cooperation for the foreseeable future.

The spin axes of *Wind* and ACE are orthogonal to each other, which provides a very useful opportunity for magnetic field cross-calibration. The spin plane components of fluxgate magnetometers are the most accurate, so the two spacecraft use the orthogonality of their spin planes to their advantage during periods when the two spacecraft are in near proximity to each other.

ACE has a much more robust and wider coverage of energies for high energy particle observations. However, the EPACT-LEMT telescope on *Wind* can observe particles in the ∼1–10 MeV/nuc range, which falls between the ULEIS and SIS detectors on ACE. Further, the ecliptic south spin axis of *Wind* allows the LEMT telescope to determine anisotropies in the

high energy particles (e.g., it can detect particles streaming sunward from the outer heliosphere). Finally, the larger geometric factor of EPACT allows it to observe less intense solar energetic particle events.

**In summary, *Wind* provides significant and unique calibration information for ACE, complements its measurements and facilitates collaborative, multi-spacecraft studies.**

**DSCOVR**

The Deep Space Climate Observatory (DSCOVR) was launched on Feb. 11, 2015. DSCOVR is tasked to provide solar wind proton and magnetic field measurements from L1 (the same region where *Wind*, ACE and SOHO operate) for NOAA space weather prediction purposes.

*Wind* has been an essential calibrator for DSCOVR and is the primary reference for DSCOVR plasma data trending and anomaly tracking. The DSCOVR PlasMag Faraday Cup (FC) is a plasma diagnostic instrument of central importance to real time space weather monitoring, modeling, and forecasting efforts. The sensor is physically identical to the *Wind* SWE FCs in most respects and operates in a similar mode, but it is perpetually sun-pointed. In 2015–2016, during the extended commissioning period for the instrument, grounding and charging anomalies threatened to render the DSCOVR instrument unusable. *Wind* SWE measurements of solar wind protons were used as a standard for a full recalibration of the DSCOVR FC response, a characterization of the anomalous backgrounds, and a revision of the operating mode such that it could meet requirements.

As DSCOVR has been accepted and transitioned to space weather operations, the *Wind* spacecraft continues to provide the standard against which the DSCOVR measurement consistency and quality are evaluated. Properly calibrated, the relatively high cadence measurements from both the FC and the magnetometer on DSCOVR provide an interesting compliment to the *Wind* measurements. The *Wind*-DSCOVR comparison also constitutes a new baseline for multi-point studies of solar wind structures near L1, completing a tetrahedral solar wind constellation with SOHO and ACE that is suitable for planar timing analysis on scales comparable to the solar wind correlation scale [e.g., *Weygand et al.*, 2009]. Public release of science-grade data from DSCOVR began in late 2016, enabling joint *Wind*-DSCOVR investigations to begin.

**STEREO**

With the recent return of communications with STEREO-Ahead after passing behind the sun and the interrupted communications with STEREO-Behind, *Wind* continues to be one of only three inner heliospheric missions with radio observations of the sun (i.e., *Wind*, MAVEN, and STEREO-Ahead). With the ending of MESSENGER in April 2015 and VEX in January 2015, *Wind*'s importance in global heliospheric observations has greatly increased. Until the recovery of STEREO-Behind, *Wind*, MAVEN, and STEREO-Ahead will be the only inner heliospheric radio observatories (though radio bursts need to be very strong to be observed by MAVEN). With the current non-viability of STEREO-Behind, *Wind* is acting as the stereo-partner of STEREO-Ahead for current studies particularly because of the similarities in their instrumentation. **Thus, *Wind* continues to be and will remain a critical component in the HSO.**

**MAVEN**

The Mars Atmosphere and Volatile EvolutioN Mission (MAVEN), designed to study the Martian atmosphere, arrived at Mars (∼1.5 AU) on September 22, 2014. Mars remained on the far side of the sun, relative to Earth, until early 2016. It is currently ∼90° from Earth. Thus, *Wind*, MAVEN, and STEREO-Ahead form a unique constellation currently spanning ∼180° allowing for in–situ plasma and remote radio measurements of large transients in the inner heliosphere for both observational and simulation studies of space weather.

## 4.2 Solar Probe Plus and Solar Orbiter

*Solar Probe Plus* (SPP) and *Solar Orbiter* (SolO) are not planned to launch until 2018, thus their primary mission starts during the second half of this proposal period. Even so, *Wind* continues to produce significant and relevant studies helping to improve the future science output and predictions/tests for these two flagship missions. Only the high resolution of *Wind* measurements can provide an appropriate 1 AU baseline for SPP and SolO observations. DSCOVR is expected to exhaust its propellant after ∼5 years and has limited measurements (i.e., only magnetic fields and thermal ions). For comparison, *Wind* has >50 years of fuel. The short ∼88 day orbit of SPP and the ∼0.3–0.76 AU orbit of SolO will provide frequent radial and magnetic alignment with *Wind* allowing for multi-spacecraft studies. This will significantly enhance the science return of both SPP and SolO.

The primary scientific goal of SPP is to determine the processes responsible for heating and acceleration of the solar corona and solar wind. These processes (e.g., instabilities, wave-particle interactions) tend to take place on very small time scales near the Sun; barely resolvable even by the extremely high cadence SPP instruments. However, near 1 AU, the same processes operate slower making their observa-

tion by *Wind* possible. Towards the next solar maximum particle and plasma observations from *Wind*, SPP, and SolO, during periods when all three spacecraft are radially or magnetically aligned, will allow researchers to study the radial variation of particle acceleration at interplanetary shocks, of the transport coefficients governing the propagation of solar energetic particles, and the evolution of the magnetic turbulence in the solar wind from 10 $R_\odot$ to 1 AU.

**Thus, *Wind* will continue to help identify local vs. remote heating and acceleration processes, complementing the observations of *Wind* and STEREO-A/B during the past solar cycle for longitudinal variations of plasma and energetic particle observations, and will contribute essential to both SPP and SolO.**

## 4.3 IBEX and *Voyager*

*Wind* observations have usually supplied the 1 AU baseline for deep space observations (e.g., the two Voyager spacecraft) since the IMP 8 magnetometer stopped returning data in 2000. **The robust and continuous solar wind measurements from *Wind* are essential for studies ranging from the predicted position of the termination shock and heliopause**, also observed remotely by IBEX, **to the evolution of solar wind transients from the inner-to-outer heliosphere.**

## 4.4 Magnetospheric Missions

Nearly all magnetospheric investigations utilize, in some way, data from an upstream solar wind monitor. This is partly evidenced by the **>1,825,000 access requests** registered by CDAWeb (>350,000 for HTTP and >1,450,000 for FTP access) for *Wind* and OMNI data (which largely relies upon *Wind* and ACE measurements) between Jan. 1, 2015 and Jan. 1, 2017. Missions that have, continue to, and will rely upon *Wind* for solar wind data include *Cluster*, THEMIS, ARTEMIS, *Van Allen Probes* and MMS. Therefore, *Wind* will remain a crucial element in magnetospheric studies through 2017.

**THEMIS**

The two THEMIS spacecraft in permanent lunar orbits, called ARTEMIS, spend a large fraction of their time in the ambient solar wind. This allows for high quality multi-spacecraft solar wind studies, e.g., determining the large-scale structure of interplanetary shocks [*Kanekal et al.*, 2016].

All five THEMIS spacecraft are equipped with high cadence (∼3s in burst mode) plasma distribution function observations allowing for very precise, multi-spacecraft studies. *Wind* provides a critical monitor of the interplanetary environment for interpretation of THEMIS measurements. For instance, the recent discovery of relativistic electrons generated locally within the ion foreshock [*Wilson III et al.*, 2016] relied heavily on *Wind* radio and energetic particle observations to rule out a solar source.

It is worth noting that THEMIS used *Wind* to calibrate its thermal plasma instruments [*McFadden et al.*, 2008a,b], since its electric field receivers could not consistently observe the upper hybrid line.

***Van Allen Probes* and MMS**

The two *Van Allen Probes* and the four MMS spacecraft launched on August 30, 2012 and March 13, 2015, respectively. Both of these missions rely heavily upon solar wind monitors for various reasons (e.g., determining the distance to the magnetopause from MMS) as evidenced by the increasing *Wind* publications per year (i.e., >330 in 2016 alone). Further, the *Van Allen Probes* Science Working Group identified a need for solar wind observations to achieve its scientific objectives. **Thus, *Wind* will continue to provide high quality solar wind observations required for the numerous magnetospheric studies by the *Van Allen Probes* and for the MMS missions.**

## 4.5 Solar and Astrophysics

**Solar Flares**

During it's more than 22 year-long history, the KONUS instrument onboard *Wind* has accumulated an unique volume of solar flare observations in the hard X-ray and gamma-ray range. Data on solar flares registered by KONUS in the triggered mode are published online (http://www.ioffe.ru/LEA/kwsun/). This database (named KW-Sun) provides light curves with high temporal resolution (up to 16 ms) and energy spectra over a wide energy range (now ∼20 keV to ∼15 MeV). The high time resolution of KONUS allows for the study of fine temporal structure in solar flares; and the KONUS energy band covers the region of non-thermal emission from electrons and ions in solar flares, that allows probing their acceleration mechanisms. New solar observations will be added to the database as soon as they arrive. The list of KONUS triggered-mode solar flares from 1994 till present time, along with their GOES classification, is automatically updated and available at http://www.ioffe.ru/LEA/Solar/.

**RHESSI**

RHESSI provides imaging and spectroscopy of the hard X-ray/$\gamma$-ray continuum and $\gamma$-ray lines emitted by energetic electrons and ions, respectively. *Wind* complements RHESSI's observations using remote observations of radio (WAVES) and $\gamma$-rays (KONUS) in addition to in–situ measurements of energetic particles (3DP, SMS, and EPACT). Thus, *Wind* can pro-

vide a secondary remote and primary in–situ observatory of solar flares and the associated energetic particles, respectively. *Wind* will continue to support this and similar RHESSI research projects.

***Swift* and *Fermi***

Cosmic gamma ray bursts (GRBs) are the brightest electromagnetic events known to occur in the universe, occurring transiently from the collapse of massive stars or coalescence of compact objects (e.g., two neutron stars or a neutron star-black hole merger) in the early universe. GRBs consist of an initial flash of gamma-rays lasting from milliseconds to minutes followed by a longer duration "afterglow" at radio and optical wavelengths. About 120 per year are detected by KONUS (almost 3000 to date).

Soft gamma repeaters (SGRs) are strongly magnetized Galactic neutron stars (surface fields up to $10^{14}$ G) that emit large bursts of X-rays and gamma-rays at irregular intervals. There are presently only about two dozen known SGR sources. When they become active they emit bursts from a few times up to hundreds of times over spans from days to months.

SGR Giant Flares (GFs) are of greater apparent intensity than GRBs and are very rare, averaging once per decade. Only a handful have been detected to date, and their intensities are sufficient to create easily detectable ionospheric disturbances; indeed KONUS has detected both GFs from SGR 1900+14 and SGR 1806-20. KONUS has also detected a GF from the Andromeda Galaxy.

KONUS was designed to study GRBs, SGRs, and GFs, with omnidirectional, unocculted sensitivity. It also has broadband sensitivity, coupled with excellent time- and energy resolution. For over two decades, it has been a key component of the Interplanetary Network (IPN, http://ssl.berkeley.edu/ipn3/index.html), maintained by Dr. Kevin Hurley, which determines the source directions of transients by triangulation. The primary spacecraft involved in the IPN are *Wind*, *Mars Odyssey*, INTEGRAL, RHESSI, *Swift*, and *Fermi*. KONUS extends the energy range of *Swift* from 150 keV to 10 MeV, a crucial data set for a global understanding of gamma-ray transients, and detects events which are Earth-occulted to *Fermi*. In addition it is generally the most sensitive of the IPN detectors to SGRs (∼350 detections to date), due to its lack of collimation and Earth occultation, and broad energy coverage.

KONUS remains a very active partner in the Gamma-ray Burst Coordinates Network or GCN (https://gcn.gsfc.nasa.gov), maintained by Dr. Scott Barthelmy (NASA-GSFC). The GCN circulates information on bursts rapidly to thousands of astronomers worldwide, who conduct multi-wavelength, and now, also neutrino and gravitational wave follow-up observations. Indeed, with the first detection of gravitational radiation by LIGO in 2016, KONUS and the IPN have taken on a new role – the search for gamma-ray transients associated with gravitational wave sources, such as the inspiral of two neutron stars in a binary system. As LIGO's sensitivity increases over the coming years, the first such detection becomes increasingly likely, ushering in a new era of astrophysical observations. As high energy neutrino detections are now becoming more common, a similar symbiosis exists for them. Thus, the instrument remains a unique, active, and irreplaceable contributor to the astrophysical community. **Due to the rarity of these astrophysical events, an additional two years of *Wind* KONUS observations will significantly enhance the events collected by *Swift*, *Fermi*, the IPN, and the GCN.**

## 4.6 *Wind*, CCMC, and CDAW

The Coordinated Community Modeling Center (CCMC) is tasked to validate heliophysics models. In particular, terrestrial magnetospheric models are driven by solar wind input. The accuracy of this input, especially during extreme solar wind conditions, is critical for the proper evaluation of the models. Historically, *Wind* measurements have been used as the standard. It is expected that as the complexity increases in future models, their sensitivity to the uncertainties of driving conditions will increase. **Thus, *Wind* measurements will continue to be an essential input for the CCMC model validation program.**

***Wind* and CDAW Data Center**

The CDAW Data Center is a repository of CMEs, radio bursts, and associated phenomena related to space weather (https://cdaw.gsfc.nasa.gov). The Data Center provides an online catalog of all CMEs, manually identified from SOHO/LASCO images since 1996, and all type II radio bursts observed by *Wind*/WAVES (link found on *Wind* webpage and in Appendix A) with links to the corresponding CMEs that produced the type II bursts. There are also daily movies that combine SOHO/LASCO images with *Wind*/WAVES dynamic spectra to identify the connection between CMEs and Type II, III, and IV radio bursts (e.g., Dynamic Movie Creator). The small subset of Type II producing CMEs have been found to play a critical role in space weather [e.g., *Vasanth et al.*, 2015] and solar energetic particles (SEPs), which is why there is another catalog associating SEPs and radio bursts. **Thus, *Wind* remains an active partner in the CDAW Data Center.**

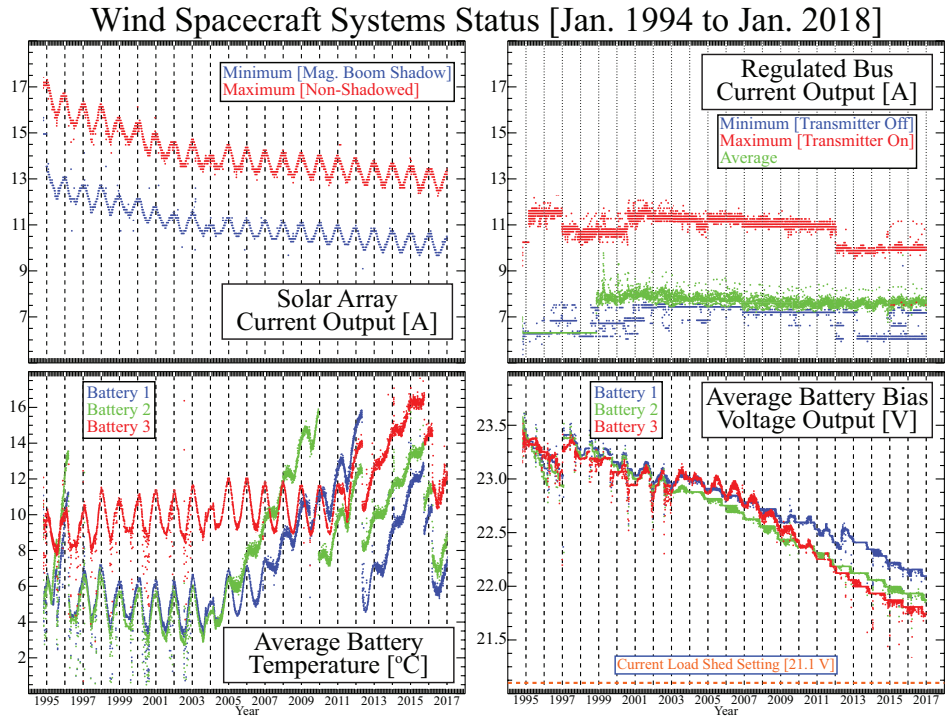


**Figure 16:** ***Summary of Wind's Status:*** *The Wind spacecraft systems status plotted from Jan. 1, 1994 to Jan. 1, 2018. The figure shows the solar panel array (upper left) current [Amp] output, regulated (upper right) bus current [Amp], average battery (lower left) temperatures [° C], and average battery (lower right) bias voltage [Volts] versus time. Each data point represents a daily average.*

# 5 Technical Implementation

## 5.1 Spacecraft Health

*Wind* continues to operate in good health. The communication system was successfully reconfigured in 2000 to enhance the telemetry margins and reliance on a single digital tape recorder (with two tape units) since 1997 has never hindered operations. The flight operations team (FOT) took steps to minimize wear and extend the lifespan of the two tape units. Since the last Senior Review, the spacecraft has experienced the usual instrument latch-ups and single-event upsets (SEUs) that are likely caused by high energy particles. As in the past, the FOT was able to restore all instruments to fully operational within a day or two depending on Deep Space Network (DSN) scheduling. The automation of the recovery process for the WAVES instrument after latch-ups (i.e., due to SEUs) was successfully completed in October 2016 and the spacecraft command tables now include automated tests of the SWE electron instrument. Thus, *Wind* continues to maintain a fully operational status.

On Oct. 27, 2014 at 21:59:38 GMT, the *Wind* command and attitude processor (CAP) suffered two simultaneous SEUs. The redundant nature of the *Wind* spacecraft bus allowed the FOT to successfully switch to a second CAP, CAP2. The FOT began the recovery of CAP1 on Jan. 21, 2015 and finished Jan. 30, 2015. Thus, the *Wind* spacecraft was fully recovered at ∼17:50 UTC on Jan. 30, 2015.

The CAP1 anomaly resulted in a complete loss of data from October 27, 2014 until November 7, 2014 (i.e., 11 days or ∼3% annual total) and partial loss from all instruments between November 7–20, 2014 (i.e., 14 days or ∼4% annual total). The SWE instrument suffered complete data loss between October 27, 2014 and November 26, 2014 (i.e., 30 days or ∼8% annual total) and partial loss (HK only) from October 27, 2014 to December 1, 2014 (i.e., 35 days or ∼10% annual total). During the recovery process between Jan. 28–30, 2015 while CAP1 was in control, the attitude/telemetry information was invalid for ∼4 hrs 41 mins (i.e., <5% of those four days).

On April 11, 2016 one of the two tape units (TUA) began experiencing issues related to the read/write head causing ∼few percent data loss per day. The flight operations team successfully switched the primary record unit to TUB on May 6, 2016 to extend the life of TUA and reduce data loss. *Wind* continues to average >98% data recovery rates and the TUB status is fully operational.

An examination of the spacecraft power systems (see Figure 16) shows that the batteries can maintain average bias voltages high enough to exceed the

current load shed setting of 21.1 V until at least mid ∼2027 (i.e., extrapolation to yellow line in lower right-hand panel). To cause a spacecraft reset, all three batteries must simultaneously fall below this commandable voltage level. The load shed setting is commandable from ground and will be changed when necessary to avoid a spacecraft reset. We can safely reduce the load shed setting down to at least 19.6 V, which corresponds to at least four more years (beyond ∼2027) without issue.

Since the last Senior Review, all three batteries went through two mode changes to reduce the maximum charge voltage (see lower-left-hand panel in Figure 16). Each battery was experiencing excess charging, causing an increase in temperature and reduction in efficiency. The successful mode changes reduced the temperatures to nominal ranges. At least one of the three batteries will require another mode change in late ∼2020. At this rate – ∼3 years between mode changes – the batteries will last another ∼15–18 years since there are currently 5 more mode levels available before other alternatives are required.

The solar array output is producing more than enough current for spacecraft operations and will continue to do so well past the year ∼2018; assuming a requirement that a minimal current be drawn from the batteries (i.e., blue line in upper left-hand panel remains higher than red line in upper right). However, *Wind* operated for over a decade not satisfying this requirement, when in early 2012 a more efficient sequence of commands were implemented during transmission. Under this less conservative requirement and the current rate of degradation, the solar arrays would no longer meet the minimum current requirements for the regulated bus output by the late 2040's (i.e., when the blue line in upper left-hand panel drops below the green line in upper right). Therefore, *Wind* can operate at current capacity well into the next decade.

*Wind* continues to maintain a large fuel reserve showing ∼54 kg remaining, which is equivalent to ∼103 m/s of radial delta-V assuming normal thruster operations. *Wind* need only perform ∼4 station keeping maneuvers each year, each of which only require ∼0.2–0.5 m/s delta-V. Thus, *Wind* has enough fuel for >50 years.

## 5.2 Instrument Status

Seven of the eight *Wind* instruments, including all of the fields and particles suits, remain largely or fully functional. The only instrument turned off is the TGRS $\gamma$-ray instrument that was designed for only a few years of operations. The general status of all instruments is summarized in Table 3.

The specific degradations in instrument capabilities are the following: EPACT-IT detector failed and the EPACT-APE detector only returns two energy channels of ∼5 and ∼20 MeV protons during enhanced periods. The LEMT and STEP telescopes of the same instrument continue to operate normally, providing crucial and unique observations of solar energetic particles up to 10 MeV in energy. The SMS-SWICS solar wind composition sensor had to be turned off in May 2000. The SMS DPU experienced a latch-up reset on 26 June 2009 that placed the MASS acceleration/deceleration power supply into a fixed voltage mode, rather than stepping through a set of voltages. It has been determined that a moderate risk power cycling of the SMS DPU would be required to fix this problem. In order to protect the unique and fully functional STICS sensor, it has been decided to leave the MASS sensor in a fixed voltage mode that allows reasonable but reduced science data collection. In 2010, MASS experienced a small degradation in the acceleration/deceleration power supply which reduced the efficiency of the instrument, though this does not seriously affect science data analysis.

The VEIS thermal electron detectors on the SWE instrument experienced high voltage problems in November, 2001. This problem was resolved by reprogramming the SWE Strahl sensor to recover most of the original functions. Moreover, the 3DP instrument also covers the impacted electron measurements making these observations still redundant and hence robust. The entire SWE instrument suite required a full reset due to the CAP anomaly (see Section 5.1 for details), which resulted in a complete loss of data from late Oct. 27, 2014 to Nov. 26, 2014, and partial loss until Dec. 1, 2014 when the instrument was returned to nominal operations.

On May 2014 the 3DP instrument (specifically PESA Low) suffered an anomaly that only affected the telemetry house keeping (HK) data. A quick investigation showed that while the telemetry information (e.g., micro-channel plate grid voltage) showed unreliable instrument operations information, the science data remained unaffected (i.e., no noticeable change in flux was observed during and after event). All the other detectors within the 3DP instrument suite continue to operate nominally. Thus, the anomaly resulted in no loss of scientific data.

Aside from the complete or partial data losses due to the 2014 CAP and 2016 tape unit anomalies (see Section 5.1 for details), all of the instruments continue to be fully functional.

## 5.3 Science Team

The *Wind* instrument/science team is very small but an extremely dedicated group of scientists. Due to the longevity of the mission, a number of the origi-

**Table 3:** The status of the *Wind* instruments

| Instrument | Principal Investigator | Institution | Status |
|---|---|---|---|
| **SWE** | A.F- Viñas (acting) | Electrons: GSFC, UNH<br>Ions: SAO | Strahl detector reconfigured<br>Faraday Cup fully operational |
| **3DP** | S.D. Bale | UC Berkeley | Fully operational |
| **MFI** | A. Szabo | GSFC | Fully operational |
| **SMS** | S. Lepri | U. Michigan | SWICS turned off<br>MASS reduced coverage<br>STICS fully operational |
| **EPACT** | L.B. Wilson III (acting) | GSFC | IT turned off<br>APE – only 5 and 20 MeV protons<br>LEMT and STEP operational |
| **WAVES** | R. MacDowall | GSFC | Fully operational |
| **KONUS** | R. Aptekar | Ioffe Institute, Russia | Fully operational |
| **TGRS** | B. Teegarden | GSFC | Intentionally turned off<br>(ran out of coolant) |

nal instrument PIs have retired or passed away. Keith Ogilvie passed the leadership of the SWE instrument suite to Adolfo Viñas (GSFC) and Justin Kasper (University of Michigan) leading the SWE Faraday Cup team. Stuart Bale has taken over as PI of 3DP at the University of California, Berkeley. Adam Szabo (GSFC) is the PI for the MFI instrument. Sue Lepri (University of Michigan) is the PI for SMS. Both the original and previous acting EPACT PIs, Tycho von Rosenvinge and Allen Tylka, respectively, recently retired so Lynn B. Wilson III (GSFC) and John F. Cooper (GSFC) are currently performing the duties of the EPACT PI until a suitable replacement can be found. Finally, Dr. Wilson was promoted to Project Scientist for *Wind* in June 2016. The new team brings a great deal of experience and enthusiasm for new discoveries, as evidenced by the long and increasing list of *Wind* scientific publications (i.e., **over 600 refereed publications** since the last Senior Review). There are also several new data sets that have been released since the last Senior Review and some to be released before the next Senior Review resulting from efforts by the new team members (e.g., see Appendix A).

**Students**

*Wind* remains a very popular source of solar wind measurements and a rich source of material for Masters, PhD, and postdoctoral work. Since the last Senior Review, 13 students earned PhDs, 3 students earned Masters degrees, and 4 postdocs benefited from *Wind* observations. There are currently 16 PhD and 4 Masters students (of which we are aware) using *Wind* observations. The university team members also rely on a large number of undergraduate interns to increase their scientific productivity.

## 5.4 Ground Operations

*Wind* ground operations take place at Goddard and is fully transitioned from the legacy *Polar-Wind-Geotail* system to Multi-Mission Operations Center (MMOC) that consolidates *Wind* operations with that of ACE. This transition became necessary with the decommissioning of Polar on April 30, 2008 and it includes the upgrade of outdated and costly to maintain hardware and software. *Wind* operations were moved to the MMOC on March 11, 2010 with the MMOC Operational Readiness Review held on March 30, 2010.

For cost saving measures, the flight operations team reduced staffing by 1 FTE in November 2008 and modified shift schedules to reduce operational coverage from twelve to eight hours (reducing the need for overtime and shift differential). With the successful transition of *Wind* flight operations into the MMOC, the staffing levels have been reduced to operate the ACE and *Wind* missions with a combined team that also includes non-traditional flight operations skills (HW/SW maintenance, Flight Dynamics attitude analysis). Re-engineering/upgrading existing systems promoted efficiency with respect to implementing IT Security and HW/ SW maintenance as well as system administration. Automation is being implemented with a unified approach to further increase efficiency (e.g., SWE electron instrument auto-recovery and WAVES recovery after latch ups). The teams will continue to cross train at multiple positions so that prime and backup roles are covered. In spite of the disruptions due to the 2014 CAP and 2016 tape unit anomalies, the data recovery rate for *Wind* for the years 2015 and 2016 averaged ∼96.8% and ∼98.4%, respectively. Since the recovery from the 2016 TUA anomaly, the median daily data recovery rate has been >99%. Most of the unrecoverable data

loss occurred when *Wind* Deep Space Network (DSN) supports were released for other spacecraft launches and emergencies with some data loss resulting also from network problems.

The current operation of *Wind* requires one ∼2 hour DSN support every other day, though contacts occur more frequently sometimes. This allows the uplinking of the Stored Command Table load and the playback of the Digital Tape Recorder (DTR). *Wind* also maintains real-time solar wind monitoring during these 2 hour contacts. In 2001, an attempt was made to reduce the number of DSN contacts, and hence the cost of operations, by scheduling DSN time only once every three days, albeit for longer durations. Reducing the number of contacts saves the lengthy setup and reset times. After extensive testing it was concluded that this scenario did not provide significant savings and introduced critical risks to the mission. *Wind* can store only three days worth of commands, thus this is the longest *Wind* can go without ground contact or the spacecraft performs an emergency load shed. Hence the current flexibility to negotiate contact time with DSN would be eliminated. Also, all of these infrequent contacts would be fully attended regardless of the time of day. Currently about half of the contacts are completely automated allowing the operation staff to keep day schedules. Thus, the current daily contact scenario is considered optimal. It should be noted that all DSN and communication costs are reported as "In Kind" costs so they are not considered part of *Wind*'s operational budget.

The automated distribution and archiving of level zero files and production of key parameter (KP) files takes place at Goddard in the Science Directorate under the control of the project scientist. The two server (plus backup) system are periodically upgraded and maintained at modest cost.

# 6 In-Guide Budget

The in-guide budget described in this section will fund the mission operations necessary to continue the safe operation of the *Wind* spacecraft along with basic data reduction and validation processes performed at the various instrument institutions. As in past Senior Reviews, nearly all of the scientific research outlined in the previous sections are expected to be or were funded through external sources, e.g., the ROSES GI and SR&T programs (or other opportunities) with each element individually proposed and peer reviewed. The only funding allocated for scientific research in *Wind*'s budget occurs indirectly as a result of funding the instrument teams to process and validate the data.

## 6.1 Mission Operations

The inputs in the budget spreadsheet Table 11 show the direct and indirect costs for the *Wind* mission. The "Labor" line includes all civil servant labor dollars resulting from the "FTE 1" and "FTE 2" lines. The "Travel" line includes only travel dollars used by Code 670 for *Wind*-related meetings/conferences. The "Mission Operations" section includes all direct costs for flight operations and attitude/orbit support. The "Data Analysis" section includes all costs funded directly through GSFC. The "Total Uncosted" section shows the expected eight weeks of uncosted carryover funds through the end of the fiscal year. The last section shows "In-Kind" costs that are indirect costs funded by other sources. Below we explain the costs included in each line of the budget spreadsheet.

The total shown in the first line of the "Mission Operations" section includes the 5.6 WYEs for the FOT (i.e., "WYE 1" line) for FY18–FY22. It also includes support from flight dynamics for orbit determination and station keeping maneuvers and the DSN scheduling work. The sustained engineering costs for FY18–FY22 are for system administration of the MMOC, updates to spacecraft commands, hardware and software updates, and level zero file processing. The civil servant labor for a Mission Director (i.e., "FTE 1" line) is charged at 0.2 FTE and the dollar amount is included in the "Labor" line near the top.

The "Data Analysis" section includes all science operations for the *Wind* project including on-site contractor labor (i.e., itemized in the "WYE 2" line), funding for a resource analyst at 0.2 WYE, and all instrument operations costs. All civil servant labor dollars are not included here but shown in the "Labor" line near the top of the spreadsheet but are itemized by time in the "FTE 2" line. The totals for "FTE 2" include: maintaining the *Wind* portion of the reengineered PWG system by a software engineer at 0.2 FTE; 0.5 FTE for the project scientist; and 0.2 FTE for data production and calibration split between the SWE (electron) and EPACT instruments. The PWG system – responsible for the archival of the level zero data and its distribution to the instrument sites and for the generation of the quick-look key parameter (KP) data files – requires ∼$30k/year for hardware (e.g., replacement hard drives) and software license fees. The remaining costs are distributed among the university-led instrument teams. Note that ∼33% of the in-guide funding is needed for mission operations and only ∼6% for project management. Thus, more than half of the *Wind* budget still goes to the instrument teams for data processing and validation. The cost of the recent transition of the *Wind* pri-

mary recorder from tape unit A (TUA) to TUB, will be attempted to be absorbed in the existing small funding level.

The "In-Kind costs to mission" line includes services provided to *Wind* that are funded by other sources (e.g., SCAN). These costs are allocated to *Wind*, but are not supported with project funds. This line includes costs for mission communication services (e.g., voice and data connections at GSFC) and supplemental costs for flight dynamics and flight operations support. The "Space Communications Services" line shows all DSN costs. Again, these costs are not supported with project funds.

## 6.2 Data Production and Accessibility

The *Wind* science data products are publicly served directly from the instrument team sites (most are directly available from CDAWeb), with a single project webpage containing links to and descriptions of the large number of *Wind* data products (https://wind.nasa.gov). *Wind* is also an active participant in the development of the Virtual Heliophysics Observatory or VHO (https://vho.nasa.gov) that makes data queries even more user friendly and powerful. Details of the data production are given below.

Over half of the requested in-guide funding is allocated to the generation, calibration, and validation of the various *Wind* instrument data products. After receiving the level zero instrument data along with housekeeping and ephemeris information, the instrument teams are responsible for the generation of science quality data that is fully calibrated and validated typically through the performance of well established scientific analysis. The instrument teams are required to provide complete documentation and intermediate-term archiving prior to final submission to SPDF/CDAWeb. In addition, the occasional ($\sim$4/year) station keeping maneuvers necessitate instrument level commanding that the instrument teams are required to support. Thus, besides data production expertise, the teams have to maintain a low level engineering capability that can support routine and emergency operations. Finally, since *Wind* does not have a project level science center, the instrument teams are responsible for the public dissemination of their data through the maintenance of local webpages and final submission to SPDF/CDAWeb.

Due to the limited funding available, the instrument teams optimized their processes to stay within $\lesssim$1 FTE for all aspects of operation. All fully functional instruments (MFI, SWE/Electron, SWE/Faraday Cup, WAVES, 3DP, and EPACT) are allocated nearly the same amount of support, regardless of whether they are full cost accounted Goddard civil service or university-led teams. It should be noted that SWE is composed of two independent instruments: the Goddard electron instrument and the SAO/University of Michigan Faraday Cup.

The SMS instrument team receives roughly half as much due to the reduced data production requirements resulting from the SWICS failure early in the mission and partial functioning of the MASS detector (STICS is fully operational). However, STICS still continues to produce valuable and unique data, therefore continued support at this reduced level is still requested. The TGRS instrument was intentionally turned off after it ran out of coolant (this was expected and part of the design), thus has not received funding for over 15 years. Finally, the astrophysical KONUS instrument receives no heliophysics funding. This instrument receives some minor amount of funding in Russia for data production and even less support from the Gamma-Ray Coordinates Network (GCN) – currently funded through High Energy Astrophysics Science Archive Research Center (HEASARC) – for minimal effort by a Goddard civil servant for data processing. Thus, no new funding is requested for them in this proposal. All of these costs, except civil servant salaries, are included in the "Data Analysis" section of Table 11.

The current *Wind* project funding level does not allow any significant amount of funded science research and most of the results presented in this proposal were generated through independent funding (e.g., ROSES proposals). However, the core data calibration and validation work carried out by the individual instrument teams does require some amount of science data analysis to verify the accuracy of the generated data products. It is difficult to be quantitative about the fraction of work involved in this data validation work because it arises indirectly from the calibration and validation of the instrument data. However, we can estimate an upper bound by summing the total labor costs for instrument team scientists-only (i.e., excluding overhead and engineer/technician and resource analyst salaries) finding that $\sim$13% of the total *Wind* funding can be attributed to science data analysis or $\sim$20% of the non-mission operations funding. Again, these are very conservative estimates and all result indirectly from the normal calibration and validation of the instrument data.

# *References*

Adrian, M. L., et al. (2016), Solar Wind Magnetic Fluctuations and Electron Non-thermal Temperature Anisotropy: Survey of Wind-SWE-VEIS Observations, *Astrophys. J.*, *833*, 49, doi:10.3847/

1538-4357/833/1/49.

Agueda, N., et al. (2014), Release timescales of solar energetic particles in the low corona, *Astron. & Astrophys.*, *570*, A5, doi:10.1051/0004-6361/201423549.

Altobelli, N., et al. (2016), Flux and composition of interstellar dust at Saturn from Cassini's Cosmic Dust Analyzer, *Science*, *352*, 312–318, doi:10.1126/science.aac6397.

Bale, S. D., et al. (2009), Magnetic Fluctuation Power Near Proton Temperature Anisotropy Instability Thresholds in the Solar Wind, *Phys. Rev. Lett.*, *103*, 211,101, doi:10.1103/PhysRevLett.103.211101.

Bougeret, J.-L., et al. (1995), Waves: The Radio and Plasma Wave Investigation on the Wind Spacecraft, *Space Sci. Rev.*, *71*, 231–263, doi:10.1007/BF00751331.

Burgess, D., et al. (2012), Ion Acceleration at the Earth's Bow Shock, *Space Sci. Rev.*, *173*, 5–47, doi:10.1007/s11214-012-9901-5.

Chen, C. H. K., et al. (2016), Multi-species Measurements of the Firehose and Mirror Instability Thresholds in the Solar Wind, *Astrophys. J. Lett.*, *825*, L26, doi:10.3847/2041-8205/825/2/L26.

Dierckxsens, M., et al. (2015), Relationship between Solar Energetic Particles and Properties of Flares and CMEs: Statistical Analysis of Solar Cycle 23 Events, *Solar Phys.*, *290*, 841–874, doi:10.1007/s11207-014-0641-4.

Ebert, R. W., et al. (2012a), Corotating Interaction Region Associated Suprathermal Helium Ion Enhancements at 1 AU: Evidence for Local Acceleration at the Compression Region Trailing Edge, *Astrophys. J.*, *749*, 73, doi:10.1088/0004-637X/749/1/73.

Ebert, R. W., et al. (2012b), Helium Ion Anisotropies in Corotating Interaction Regions at 1 AU, *Astrophys. J. Lett.*, *754*, L30, doi:10.1088/2041-8205/754/2/L30.

Farrell, W. M., et al. (1995), A method of calibrating magnetometers on a spinning spacecraft, *IEEE Trans. Mag.*, *31*, 966–972, doi:10.1109/20.364770.

Fedorov, A., et al. (2011), The IMPACT Solar Wind Electron Analyzer (SWEA): Reconstruction of the SWEA Transmission Function by Numerical Simulation and Data Analysis, *Space Sci. Rev.*, *161*, 49–62, doi:10.1007/s11214-011-9788-6.

Filwett, R. J., et al. (2017), Source Population and Acceleration Location of Suprathermal Heavy Ions in Corotating Interaction Regions, *Astrophys. J.*, in press.

Fox, N. J., et al. (2016), The Solar Probe Plus Mission: Humanity's First Visit to Our Star, *Space Sci. Rev.*, *204*, 7–48, doi:10.1007/s11214-015-0211-6.

Gary, S. P., et al. (2016), Ion-driven instabilities in the solar wind: Wind observations of 19 March 2005, *J. Geophys. Res.*, *121*, 30–41, doi:10.1002/2015JA021935.

Gedalin, M., et al. (2016), Dependence of the Spectrum of Shock-Accelerated Ions on the Dynamics at the Shock Crossing, *Phys. Rev. Lett.*, *117*(27), 275101, doi:10.1103/PhysRevLett.117.275101.

Ghielmetti, A. G., et al. (1983), Calibration system for satellite and rocket-borne ion mass spectrometers in the energy range from 5 eV/charge to 100 keV/charge, *Rev. Sci. Inst.*, *54*, 425–436, doi:10.1063/1.1137411.

Gloeckler, G., et al. (1995), The Solar Wind and Suprathermal Ion Composition Investigation on the Wind Spacecraft, *Space Sci. Rev.*, *71*, 79–124, doi:10.1007/BF00751327.

Greiner, J., et al. (2015), A very luminous magnetar-powered supernova associated with an ultra-long $\gamma$-ray burst, *Nature*, *523*, 189–192, doi:10.1038/nature14579.

Gruen, E., et al. (1992), The ULYSSES dust experiment, *Astron. & Astrophys. Suppl.*, *92*, 411–423.

Gruesbeck, J. R., et al. (2015), Evidence for Local Acceleration of Suprathermal Heavy Ion Observations during Interplanetary Coronal Mass Ejections, *Astrophys. J.*, *799*, 57, doi:10.1088/0004-637X/799/1/57.

Hathaway, D. H. (2015), The Solar Cycle, *Living Rev. Solar Phys.*, *12*, 4, doi:10.1007/lrsp-2015-4.

Jian, L. K., et al. (2016), Electromagnetic cyclotron waves in the solar wind: Wind observation and wave dispersion analysis, in *American Institute of Physics Conference Series*, *American Institute of Physics Conference Series*, vol. 1720, p. 040007, doi:10.1063/1.4943818.

Kanekal, S. G., et al. (2016), Prompt acceleration of magnetospheric electrons to ultrarelativistic energies by the 17 March 2015 interplanetary shock, *J. Geophys. Res.*, *121*, 7622–7635, doi:10.1002/2016JA022596.

Kartavykh, Y. Y., et al. (2016), Simulation of Energetic Particle Transport and Acceleration at Shock Waves in a Focused Transport Model: Implications for Mixed Solar Particle Events, *Astrophys. J.*, *820*, 24, doi:10.3847/0004-637X/820/1/24.

Kasper, J. C. (2002), Solar wind plasma: Kinetic properties and micro- instabilities, Ph.D. thesis, MASSACHUSETTS INSTITUTE OF TECHNOLOGY, advisor: Alan J. Lazarus.

Kasper, J. C., et al. (2006), Physics-based tests to identify the accuracy of solar wind ion mea-

surements: A case study with the Wind Faraday Cups, *J. Geophys. Res.*, *111*, 3105, doi:10.1029/2005JA011442.

Kasper, J. C., et al. (2008), Hot Solar-Wind Helium: Direct Evidence for Local Heating by Alfvén-Cyclotron Dissipation, *Phys. Rev. Lett.*, *101*, 261,103, doi:10.1103/PhysRevLett.101.261103.

Kasper, J. C., et al. (2016), Solar Wind Electrons Alphas and Protons (SWEAP) Investigation: Design of the Solar Wind and Coronal Plasma Instrument Suite for Solar Probe Plus, *Space Sci. Rev.*, *204*, 131–186, doi:10.1007/s11214-015-0206-3.

Kellogg, P. J., et al. (2016), Dust impact signals on the wind spacecraft, *J. Geophys. Res.*, *121*, 966–991, doi:10.1002/2015JA021124.

Lepping, R. P., et al. (1995), The Wind Magnetic Field Investigation, *Space Sci. Rev.*, *71*, 207–229, doi:10.1007/BF00751330.

Lin, R. P., et al. (1995), A Three-Dimensional Plasma and Energetic Particle Investigation for the Wind Spacecraft, *Space Sci. Rev.*, *71*, 125–153, doi:10.1007/BF00751328.

Lionello, R., et al. (2014), Application of a Solar Wind Model Driven by Turbulence Dissipation to a 2D Magnetic Field Configuration, *Astrophys. J.*, *796*, 111, doi:10.1088/0004-637X/796/2/111.

Liu, T. Z., et al. (2016), Observations of a new foreshock region upstream of a foreshock bubble's shock, *Geophys. Res. Lett.*, *43*, 4708–4715, doi:10.1002/2016GL068984.

Malandraki, O. E., et al. (2012), Scientific Analysis within SEPServer – New Perspectives in Solar Energetic Particle Research: The Case Study of the 13 July 2005 Event, *Solar Phys.*, *281*, 333–352, doi:10.1007/s11207-012-0164-9.

Malaspina, D. M., and L. B. Wilson III (2016), A database of interplanetary and interstellar dust detected by the Wind spacecraft, *J. Geophys. Res.*, *121*, 9369–9377, doi:10.1002/2016JA023209.

Malaspina, D. M., et al. (2014), Interplanetary and interstellar dust observed by the Wind/WAVES electric field instrument, *Geophys. Res. Lett.*, *41*, 266–272, doi:10.1002/2013GL058786.

Maruca, B. A., et al. (2013), Collisional Thermalization of Hydrogen and Helium in Solar-Wind Plasma, *Phys. Rev. Lett.*, *111*(24), 241101, doi:10.1103/PhysRevLett.111.241101.

Maruca, B. A., et al. (2016), Janus: Graphical Software for Analyzing In-Situ Measurements of Solar-Wind Ions, *AGU Fall Meeting Abstracts*, pp. SH11A–2216, dec. 12-16, 2016, San Francisco, CA.

Matthaeus, W. H., et al. (2016), Ensemble Space-Time Correlation of Plasma Turbulence in the Solar Wind, *Phys. Rev. Lett.*, *116*(24), 245101, doi:10.1103/PhysRevLett.116.245101.

McFadden, J. P., et al. (2008a), The THEMIS ESA Plasma Instrument and In-flight Calibration, *Space Sci. Rev.*, *141*, 277–302, doi:10.1007/s11214-008-9440-2.

McFadden, J. P., et al. (2008b), THEMIS ESA First Science Results and Performance Issues, *Space Sci. Rev.*, *141*, 477–508, doi:10.1007/s11214-008-9433-1.

Nieves-Chinchilla, T., et al. (2016), A Circular-cylindrical Flux-rope Analytical Model for Magnetic Clouds, *Astrophys. J.*, *823*, 27, doi:10.3847/0004-637X/823/1/27.

Nieves-Chinchilla, T., et al. (2017), Understanding the internal magnetic field configurations of ICMEs using 20+ years of Wind observations, *Solar Phys.*, submitted Feb. 16, 2017.

Nitta, N. V., et al. (2015), Solar Sources of $^3$He-rich Solar Energetic Particle Events in Solar Cycle 24, *Astrophys. J.*, *806*, 235, doi:10.1088/0004-637X/806/2/235.

Ogilvie, K. W., et al. (1995), SWE, A Comprehensive Plasma Instrument for the Wind Spacecraft, *Space Sci. Rev.*, *71*, 55–77, doi:10.1007/BF00751326.

Omidi, N., and D. G. Sibeck (2007), Formation of hot flow anomalies and solitary shocks, *J. Geophys. Res.*, *112*, A01203, doi:10.1029/2006JA011663.

Reames, D. V. (1999), Quiet-Time Spectra and Abundances of Energetic Particles During the 1996 Solar Minimum, *Astrophys. J.*, *518*, 473–479, doi:10.1086/307255.

Reames, D. V. (2015), What Are the Sources of Solar Energetic Particles? Element Abundances and Source Plasma Temperatures, *Space Sci. Rev.*, *194*, 303–327, doi:10.1007/s11214-015-0210-7.

Reames, D. V. (2016a), Temperature of the Source Plasma in Gradual Solar Energetic Particle Events, *Solar Phys.*, *291*, 911–930, doi:10.1007/s11207-016-0854-9.

Reames, D. V. (2016b), The Origin of Element Abundance Variations in Solar Energetic Particles, *Solar Phys.*, *291*, 2099–2115, doi:10.1007/s11207-016-0942-x.

Reames, D. V. (2016c), Element Abundances and Source Plasma Temperatures of Solar Energetic Particles, in *Journal of Physics Conference Series*, *J. Phys. Conf. Ser.*, vol. 767, p. 012023, doi:10.1088/1742-6596/767/1/012023.

Reames, D. V., and C. K. Ng (2001), On the Phase of the 27 Day Modulation of Anomalous and Galactic Cosmic Rays at 1 AU during Solar Minimum, *Astrophys. J. Lett.*, *563*, L179–L182, doi:10.1086/338654.

Reames, D. V., et al. (2015), Temperature of the

Source Plasma for Impulsive Solar Energetic Particles, *Solar Phys.*, *290*, 1761–1774, doi:10.1007/s11207-015-0711-2.

Richardson, I. G., and H. V. Cane (2010), Interplanetary circumstances of quasi-perpendicular interplanetary shocks in 1996-2005, *J. Geophys. Res.*, *115*, 7103, doi:10.1029/2009JA015039.

Salas-Matamoros, C., and K.-L. Klein (2015), On the Statistical Relationship Between CME Speed and Soft X-Ray Flux and Fluence of the Associated Flare, *Solar Phys.*, *290*, 1337–1353, doi:10.1007/s11207-015-0677-0.

Štverák, v., et al. (2008), Electron temperature anisotropy constraints in the solar wind, *J. Geophys. Res.*, *113*, 3103, doi:10.1029/2007JA012733.

Suresh, K., and A. Shanmugaraju (2015), Investigation on Radio-Quiet and Radio-Loud Fast CMEs and Their Associated Flares During Solar Cycles 23 and 24, *Solar Phys.*, *290*, 875–889, doi:10.1007/s11207-014-0637-0.

Tan, L. C., and D. V. Reames (2016), Dropout of Directional Electron Intensities in Large Solar Energetic Particle Events, *Astrophys. J.*, *816*, 93, doi:10.3847/0004-637X/816/2/93.

Turner, D. L., et al. (2013), First observations of foreshock bubbles upstream of Earth's bow shock: Characteristics and comparisons to HFAs, *J. Geophys. Res.*, *118*, 1552–1570, doi:10.1002/jgra.50198.

Usmanov, A. V., et al. (2014), Three-fluid, Three-dimensional Magnetohydrodynamic Solar Wind Model with Eddy Viscosity and Turbulent Resistivity, *Astrophys. J.*, *788*, 43, doi:10.1088/0004-637X/788/1/43.

Vasanth, V., et al. (2015), Investigation of the Geoeffectiveness of CMEs Associated with IP Type II Radio Bursts, *Solar Phys.*, *290*, 1815–1826, doi:10.1007/s11207-015-0713-0.

Viñas, A. F., et al. (2015), Electromagnetic fluctuations of the whistler-cyclotron and firehose instabilities in a Maxwellian and Tsallis-kappa-like plasma, *J. Geophys. Res.*, *120*, 3307–3317, doi:10.1002/2014JA020554.

von Rosenvinge, T. T., et al. (1995), The Energetic Particles: Acceleration, Composition, and Transport (EPACT) investigation on the WIND spacecraft, *Space Sci. Rev.*, *71*, 155–206, doi:10.1007/BF00751329.

Wang, L., et al. (2015), Solar Wind ∼20-200 keV Superhalo Electrons at Quiet Times, *Astrophys. J. Lett.*, *803*, L2, doi:10.1088/2041-8205/803/1/L2.

Wang, L., et al. (2016), The injection of ten electron/$^3$He-rich SEP events, *Astron. & Astrophys.*, *585*, A119, doi:10.1051/0004-6361/201527270.

Weygand, J. M., et al. (2009), Anisotropy of the Taylor scale and the correlation scale in plasma sheet and solar wind magnetic field fluctuations, *J. Geophys. Res.*, *114*, A07213, doi:10.1029/2008JA013766.

Wicks, R. T., et al. (2016), A Proton-cyclotron Wave Storm Generated by Unstable Proton Distribution Functions in the Solar Wind, *Astrophys. J.*, *819*(1), 6, doi:10.3847/0004-637X/819/1/6.

Wilson III, L. B. (2016), Low frequency waves at and upstream of collisionless shocks, in *Low-frequency Waves in Space Plasmas*, *Geophys. Monogr. Ser.*, vol. 216, edited by A. Keiling, D.-H. Lee, and V. Nakariakov, pp. 269–291, American Geophysical Union, Washington, D.C., doi:10.1002/9781119055006.ch16.

Wilson III, L. B., et al. (2013), Shocklets, SLAMS, and field-aligned ion beams in the terrestrial foreshock, *J. Geophys. Res.*, *118*(3), 957–966, doi:10.1029/2012JA018186.

Wilson III, L. B., et al. (2016), Relativistic electrons produced by foreshock disturbances observed upstream of the Earth's bow shock, *Phys. Rev. Lett.*, *117*(21), 215101, doi:10.1103/PhysRevLett.117.215101, editors' Suggestion.

Wood, S. R., et al. (2015), Hypervelocity dust impacts on the Wind spacecraft: Correlations between Ulysses and Wind interstellar dust detections, *J. Geophys. Res.*, *120*, 7121–7129, doi:10.1002/2015JA021463.

Xu, X., et al. (2015), Direct evidence for kinetic effects associated with solar wind reconnection, *Nature Sci. Rep.*, *5*, 8080, doi:10.1038/srep08080.

Yu, W., et al. (2016), Small solar wind transients at 1 AU: STEREO observations (2007-2014) and comparison with near-Earth wind results (1995-2014), *J. Geophys. Res.*, *121*, 5005–5024, doi:10.1002/2016JA022642.

Zachilas, L., and A. Gkana (2015), On the Verge of a Grand Solar Minimum: A Second Maunder Minimum?, *Solar Phys.*, *290*, 1457–1477, doi:10.1007/s11207-015-0684-1.

# A Mission Archive Plan

Early in its mission, *Wind* and the other GGS spacecraft relied on a very capable and extensive science operations center, the Science Planning and Operations Facility (SPOF). The SPOF was responsible for the collecting, distribution and active archiving of all level zero (LZ) and ancillary data products. The SPOF also ran daily the instrument team provided data processing software to produce quick turnaround, publicly available data, termed Key Parameters (KPs). The SPOF also provided science planning and software maintenance services.

With the passage of time, and with reducing funding levels, the SPOF had to be turned off and most of its functions were passed on to the instrument teams and to a small operation, the *Polar-Wind-Geotail* (PWG) system, that continued to perform some LZ and KP functions. This unavoidable decentralization resulted in a degree of unevenness and disparity between the various *Wind* instrument data services. To solve this problem, key *Wind* instrument team members rallied around the new distributed Heliophysics Data Environment (HDE) concept and became funding members of the Virtual Heliospheric Observatory (VHO). The VHO provides a single point of entry for data location without the costly necessity of a dedicated science operations center. As a byproduct, *Wind* instrument data were among the first to be fully documented with the common SPASE dictionary based metadata standard thus providing the user community an even level of descriptions of instruments and data products.

**Mission Operations Center**

*Wind* ground operations takes place at Goddard and is fully transitioned from the legacy system to Multi-Mission Operations Center (MMOC) that consolidates *Wind* operations with that of ACE. This transition became necessary with the decommissioning of Polar on April 30, 2008 and it includes the upgrade of outdated and costly to maintain hardware and software. *Wind* operations were moved to the MMOC on March 11, 2010 and the MMOC Operational Readiness Review was held on March 30, 2010.

The primary responsibility of the MMOC is spacecraft commanding, trend and anomaly analysis, DSN scheduling, the maintenance of *Wind* Near-Real-Time (NRT) passes and LZ generation for each instrument and spacecraft housekeeping. In addition, the Goddard Flight Dynamics Facility provides orbit solutions to the MMOC. The MMOC, in turn, sends all of these data products daily to the PWG system.

**The PWG System**

The PWG system handles the active archiving of LZ and ancillary files and their distribution to the instrument teams and various active archives. The PWG system also performs the rapid KP data production for all instruments. It resides at Goddard with the project scientist team. The PWG system has been streamlined onto only two computers (a data server and a data processor, with hot spares) and is fully automated to eliminate the need for data technicians. The system is maintained by one civil service IT engineer at a fraction of an FTE. This system also serves as the interface to the *Wind* NRT data stream, which is real-time processed data during the daily ∼2 hour long spacecraft telemetry contact times. This NRT data is available in numerical and graphical format at: https://pwg.gsfc.nasa.gov/windnrt/.

The PWG system distributes the instrument and spacecraft housekeeping LZ files to the instrument teams via FTP. All of these LZ and orbit/attitude files are also publicly accessible at ftp://pwgdata.gsfc.nasa.gov/pub/. Only the most recent 60 days are served in uncompressed format, but the whole mission is archived in GZip compression. Even though the deep archival of these data files are handled by SPDF, the PWG system also backs up all LZ data at two physical locations and onto CDAWeb. It should be noted that the whole *Wind* mission to date requires only ∼400 GB of storage for the LZ data, so the backup requirements are not overwhelming.

At the beginning of the mission, all *Wind* instrument teams had to supply software to automatically process some portion of their data into science data products, the KP data. Even though the KP data is clearly not the highest quality data the instrument teams produce, its quick release (within 24 hours of observation) makes it a popular data product. The PWG system maintains this software library, with occasional support (as needed) from the instrument teams and automatically places all the KP data on https://cdaweb.gsfc.nasa.gov. A more detailed description of the various KP products is given at the instrument sections below.

The PWG system also keeps the Satellite Situation Center (SSCWeb) up to date with orbit information (https://sscweb.gsfc.nasa.gov). Thus, all orbit graphics generated on SSCWeb are always up to date.

**Instrument Data**

The bulk of the instrument data dissemination takes place through CDAWeb that also serves as

the *Wind* Active Archive. To aid the user community, we also developed a *Wind* project webpage (https://wind.nasa.gov) that identifies the entry point for each instrument data environment and provides some degree of common documentation. The *Wind* project webpage includes an updated list of publications and a link to the *Wind* Wikipedia webpage (http://en.wikipedia.org/wiki/WIND_(spacecraft)) that we developed. Most of the *Wind* data products can also be searched, down to the parameter level, through VHO providing rapid access to a wide range of events in the very long duration *Wind* data set. Next we detail the data product status of each *Wind* instrument.

**SWE Ions**

*Documentation:* The SWE Faraday Cup (FC) sub-system was designed to measure solar wind thermal protons and positive ions. The physical sensor is completely described in the *Space Science Reviews* article *Ogilvie et al.* [1995]. This article was also reproduced in the Global Geospace Mission book and portions of it are available through the *Wind* project webpage (https://wind.nasa.gov). The data production procedures are described by *Ogilvie et al.* [1995] with a much more detailed discussion in *Kasper* [2002]. Error analysis results are included in each FC data file, where systematic uncertainties of the measurements and calibration against other *Wind* instruments are discussed in *Kasper et al.* [2006]. All of this information and is available on the *Wind* project webpage.

*Data Products:* The PWG system, on receipt of the LZ data, immediately processes a KP data product for SWE/FC. This automated procedure uses a convected isotropic Maxwellian to fit to the reduced distribution functions collected by the FC. These ASCII data files (92 s resolution) are available to the public within 24 hours of the observations at CDAWeb (https://cdaweb.gsfc.nasa.gov). While the KP products were originally designed as browse, quick look data, the quality proved to be so high that this data product became a frequently used science level data product of the FC sub-system.

A data production algorithm was developed that employs a bi-Maxwellian fit and obtains anisotropic temperatures for protons and a separate fit for Alpha particles. The resulting data product (designated H1 by CDAWeb), also contains the simpler moment computations primarily to allow direct comparison with the ACE SWEPAM proton data. The whole mission (i.e., late 1994 – Present) has been reprocessed with this new algorithm and is available generally till 2–3 months behind real time as it requires the final calibrated MFI magnetic field data that needs several months to be computed. Finally, the reduced velocity distribution functions (designated WI_SW-ION-DIST_SWE-FARADAY) for the two FCs were released as a data product for the entire mission in March 2014. The details and documention for these data products can be found *Wind* project webpage (https://wind.nasa.gov) and at CDAWeb (https://cdaweb.gsfc.nasa.gov).

**Table 4:** Publicly Available SWE Ion Data Products

| Data Product | Cadence | Coverage | Format | Location |
|---|---|---|---|---|
| KP Protons (K0) | 92 s | 1994/11/17–Present | ASCII<br>CDF | FTPHelper[a]<br>CDAWeb[b] |
| Bi-Maxwellian (H1) | 92 s | 1995/01/01–Present[c] | CDF | CDAWeb |
| Reduced Velocity Distributions (SW-ION-DIST) | 92 s | 1994/11/15–2014/08/27[d] | CDF | CDAWeb |

[a] https://ftpbrowser.gsfc.nasa.gov; [b] https://cdaweb.gsfc.nasa.gov; [c] ∼6 month lag; [d] range at time of submission of proposal

It is also possible to obtain special proton beam fits on request from Michael Stevens (e-mail: msteven-scfa.harvard.edu) at the Harvard Center for Astrophysics. These fits are specialized in that they only treat events where there is an extra proton beam, in addition to the usual proton solar wind core and associated alpha-particle beam. The occurrence rate of such events is low enough to limit this data product on an event-by-event basis. However, the availability of such a product is very important as it allows for tests of ion/ion instabilities.

Finally, Bennett Maruca released an open-source Python GUI – funded by NASA ROSES grants – called *Janus* that allows users to interactively fit bi-Maxwellians for multiple (selectable) species to the reduced velocity distributions. The advantage of such software is that it can account for situations with multiple proton beams in addition to the alpha-particle population and even $O^{6+}$. The software and documentation can be found on GitHub at https://github.com/JanusWind/FC.

The list of publicly available data products are shown in Table 4. All of the FC data products are archived

at the SPDF active archive.

**SWE Electrons**

*Documentation:* The SWE electron sub-system consists of two electrostatic analyzers, the vector spectrometer (VEIS) and the Strahl spectrometer. They were designed to measure the solar wind electron distribution function. The sensors are fully described by *Ogilvie et al.* [1995] and the instrument description portion of this paper can also be found at the *Wind* project webpage (https://wind.nasa.gov).

Due to a high voltage supply failure the last available data from the VEIS detector is May 31, 2001. Since the Strahl detector has very similar capabilities (though it was used in a different manner at the beginning of the mission), the spacecraft instrument and on-ground data processing software were rewritten to recover the electron observations originally supplied by VEIS. The SWE *Space Science Reviews* article has been updated with these modifications and is available at the *Wind* project page along with a technical description of the new ground software algorithms. Moreover, the headers of the CDF data files have extensive documentation for each data product.

*Data Products:* There are four SWE electron data products: (1) electron moments from density to heat flux; (2) pitch-angle distributions with 30 angle and 13 energy bins; (3) reduced/averaged pitch-angle distribution data products; and (4) strahl observations. Starting on Aug 16, 2002, all of these four data products are generated by the new production software based on the reprogrammed Strahl detector measurements. In addition, the electron "moments" are no longer the result of integral moment calculations but estimated from the fitting of a single kappa distribution function to both the core and halo components.

**Table 5:** Publicly Available SWE Electron Data Products

| Data Product | Cadence | Coverage | Format | Location |
|---|---|---|---|---|
| Moments (H0) | 6–12 s | 1994/12/29–2001/05/31 | CDF | SPDF FTP[a], CDAWeb[b] |
| Pitch-angle (H4) | 12 s | 1994/11/30–2001/07/10 | CDF | SPDF FTP, CDAWeb |
| Avg. Pitch-angle (M2) | 12 s | 1994/12/28–2001/07/10 | CDF | SPDF FTP, CDAWeb |
| Strahl | 12 s | 1994/12/29–2002/08/14 | binary | SPDF FTP |
| New Moments (H5) | 12-15 s | 2002/08/16–2017/01/30[c] | CDF | SWEFTP, CDAWeb |
| New Pitch-angle (H3) | 12-15 s | 2002/08/16–2017/01/30[c] | CDF | SWEFTP, CDAWeb |
| New Avg. Pitch-angle (M0) | 12-15 s | 2002/08/16–2017/01/30[c] | CDF | SPDF FTP, CDAWeb |

[a] ftp://spdf.gsfc.nasa.gov/pub; [b] https://cdaweb.gsfc.nasa.gov; [c] range at time of submission of proposal

Except for the Strahl data, all electron data products are available through CDAWeb. The strahl data is available from the instrument webpage (http://web.mit.edu/space/www/wind/wind_data.html). The current availability of the SWE electron data products is summarized Table 5.

**3DP**

*Documentation:* The *Wind*/3DP instrument consists of six different sensors. There are two electron (EESA) and two ion (PESA) electrostatic analyzers (ESAs) covering energies from ∼5 eV to 30 keV and three arrays of double-ended solid state telescopes (SST) for electrons (SST Foil) and ions (SST Open) for energies ∼25–500 keV and ∼70–7000 keV, respectively. The ESAs measure the core solar wind and lower energy suprathermal particles while the SSTs are entirely focused on suprathermals. The instrument is fully described by *Lin et al.* [1995]. The instrument description portion of this paper is reproduced at the *Wind* project web site.

The ESAs produce much larger volumes of data than can be telemetered to ground, so they rely heavily upon onboard processing and burst modes. As a result a large number of 3DP data products were developed, some based on onboard processing and some generated on the ground. Some documentation of these data products exist at the 3DP instrument webpage (http://sprg.ssl.berkeley.edu/wind3dp/) and more documentation/notes can be found on the UMN 3DP webpage (https://github.com/lynnbwilsoniii/wind_3dp_pros/wiki). Extensive 3DP metadata can also be publicly located on VHO.

*Data Products:* As most *Wind* instruments, 3DP team has provided a KP production software to be run automatically at the PWG system. This data product contains electron and ion fluxes at seven energies for each particle and some basic moment computations and can be found at CDAWeb for the whole duration of the mission. The rest of the data products include: (1) onboard proton velocity moments (PM) with 3s resolution; (2) omnidirectional fluxes for thermal electrons (ELSP and EHSP) and ions (PLSP); (3) pitch-angle distributions for thermal electrons (ELPD and EHPD) and ions (PLPD); (4) omnidirectional

fluxes for suprathermal electrons (SFSP) and ions (SOSP); (5) pitch-angle distributions for suprathermal electrons (SFPD) and ions (SOPD); (6) onboard electron velocity moments (EM, not corrected for spacecraft potential); and (7) nonlinear fits of electron velocity distributions (EMFITS_E0, corrected for spacecraft potential).

The publicly available data products are shown in Table 6.

**Table 6:** Publicly Available 3DP Data Products

| Data Product | Cadence | Coverage | Format | Location |
|---|---|---|---|---|
| K0 | 92 s | 1994/11/01–2017/02/14[j] | CDF | CDAWeb[a] |
| PM[b] | 3 s | 1994/11/15–2016/12/31[j] | CDF | CDAWeb, Berkeley[c] |
| ELSP[d] | 24-98 s | 1994/11/15–2016/12/31[j] | CDF | CDAWeb, Berkeley |
| EHSP[d] | 24-98 s | 1994/12/20–2016/12/31[j] | CDF | CDAWeb, Berkeley |
| PLSP[d] | 24 s | 1994/11/15–2016/12/31[j] | CDF | CDAWeb, Berkeley |
| ELPD[d] | 24-98 s | 1994/11/15–2016/12/31[j] | CDF | CDAWeb, Berkeley |
| EHPD[d] | 24-98 s | 1994/12/20–2016/12/31[j] | CDF | CDAWeb, Berkeley |
| SST[e] SFSP[f] | 12 s | 1994/11/15–2016/12/31[j] | CDF | CDAWeb, Berkeley |
| SST SOSP[f] | 12 s | 1994/11/15–2016/12/31[j] | CDF | CDAWeb, Berkeley |
| SST SFPD | 12 s | 1994/11/15–2016/12/31[j] | CDF | CDAWeb, Berkeley |
| SST SOPD | 12 s | 1994/11/15–2016/12/31[j] | CDF | CDAWeb, Berkeley |
| EM[g] | 3 s | 1994/11/15–2016/12/31[j] | CDF | CDAWeb, Berkeley |
| EMFITS_E0[h] | 3–98[i] s | 1995/01/01–2004/12/31[j] | CDF | CDAWeb, Berkeley |

[a] https://cdaweb.gsfc.nasa.gov; [b] onboard proton moments; [c] http://sprg.ssl.berkeley.edu/wind3dp/;
[d] E = electron; P = proton; L = low energy; H = high energy; SP = omni directional fluxes; PD = pitch-angle;
[e] SST = solid state telescope; [f] SF = foil (electrons); SO = open (protons); [g] onboard electron moments; [h] corrected and calibrated electron moments; [i] varies depending on instrument mode; [j] range at time of submission of proposal

*New Data Products:* The current onboard electron moments (EM) suffer from effects of spacecraft charging (i.e., photoelectron contamination). Recent efforts have led to the creation of a new data product of electron velocity moments (EMFITS_E0) which have accounted for the spacecraft potential and calibrated against the upper hybrid line for total electron density. The new data product has been released to SPDF and distributed as CDF files for the entire mission. It comprises electron velocity moments – from density to heat flux – derived from nonlinear fits of the entire velocity distribution covered by EESA Low and High (i.e., few eV to ∼30 keV) at variable time resolutions depending upon instrument mode (e.g., ∼3s resolution in burst mode).

*Future Data Products:* Bennett Maruca received funding to adapt his *Janus* software to analyze the PESA Low and High velocity distributions. A preliminary beta-version is expected to be released by the end of calendar year 2017.

The 3DP team is currently working on a higher level data product that separates the three solar wind electron components – core, halo, and strahl – to produce a new publicly available dataset. The dataset would be similar to the EMFITS_E0 data product but separate moments for each of the three electron components. The delayed release of this data product (i.e., relative to the EMFITS_E0 data product) is due to the complexities involved in re-calibrating the micro-channel plate efficiency and deadtime tables for both EESA Low and High in order to more accurately determine the true spacecraft potential. These calibrations do not significantly affect the total velocity moments but can be critical for accurate separation and characterization of the tenuous halo and strahl components.

**SMS**

*Documentation:* The *Wind* SMS instrument suite is composed of three separate instruments: the SupraThermal Ion Composition Spectrometer (STICS); the high resolution mass spectrometer (MASS); and the Solar Wind Ion Composition Spectrometer (SWICS). STICS determines mass, mass per charge, and energy for ions in the energy range from ∼6–230 keV/e. MASS determines elemental and isotopic abundances from ∼0.5–12 keV/e. SWICS initially provided mass, charge, and energy for ions in the energy range of ∼0.5-30 keV/e, but it failed early in the mission and was turned off in May 2000, thus produces no data. MASS has been in a fixed voltage mode since 26 June 2009 due to a DPU latch-up, resulting in reduced science output. These instruments are fully described by *Gloeckler et al.* [1995]. The Instrument calibration is fully described by *Ghielmetti et al.* [1983] and in the PhD thesis of K. Chotoo both available at the *Wind*

project page. Additional data release notes are archived at the VHO.

*Data Products:* Until the failure of the SWICS instrument on May 27, 2000, combined SWICS and STICS KP files were generated that contain alpha particle information along with some carbon and oxygen abundances and temperatures. This data product is still publicly available from CDAWeb. The SWICS failure resulted in a significant effort to re-prioritize MASS and STICS. A new software system was developed which automates many data analysis functions previously done manually. The system first simultaneously assigns events to specific ion species, removing any overlap and using the statistical properties of the measurements to maximum advantage. It then uses these assigned events to construct phase space density distribution functions and corrects these for the effects of instrument efficiency and sampling geometry. Finally, it outputs these distribution functions, error estimates, and count rates for each ion along with many intermediate products that facilitate detailed analysis. The software can perform arbitrary time integrations of the data and can optionally use an inversion method to remove overlap among ions in the instrument measurement space.

Daily averages of the proton and alpha particle phase space density distribution functions for the whole mission is already publicly available through the *Wind* project webpage. In addition, hourly resolution STICS and MASS energy spectra for select days by request throughout the mission are available in digital and graphical formats from the University of Michigan page (http://solar-heliospheric.engin.umich.edu/mission_db/spectra.php?craft=2).

**Table 7:** Publicly Available SMS Data Products

| Data Product | Cadence | Coverage | Format | Location |
|---|---|---|---|---|
| KP SWICS+STICS | 4 hr | 1994/12/12–2000/05/27 | CDF | CDAWeb[a] |
| STICS[b] | 1 day | 1995/01/01–2007/12/31 | ASCII | *Wind* Project[c] |
| SWICS+MASS[d] | 1 hr | Select Days | ASCII | UMichigan[e] |
| STICS[f] | 1 day | 2005–2007 | ASCII | UMichigan |

[a] https://cdaweb.gsfc.nasa.gov; [b] proton and alpha-particle distribution functions; [c] https://wind.nasa.gov;
[d] energy spectra; [e] http://solar-heliospheric.engin.umich.edu/mission_db/spectra.php?craft=2;
[b] omnidirectional proton and alpha-particle distribution functions;

The publicly available data products are shown in Table 7.

*Future Data Products:* The SMS team is currently working to release an enhanced STICS dataset for the entire mission that will include full 3D distributions at 1 day, 2 hour, and adaptive (i.e., depends on count rates) time resolutions. The ions that will be included in this new dataset are: $H^+$; $He^+$ and $He^{2+}$; $C^+$, $C^{5+}$, and $C^{6+}$; $O^+$, $O^{6+}$, and $O^{7+}$; and $Fe^{8+}$, $Fe^{9+}$, $Fe^{10+}$, $Fe^{11+}$, $Fe^{12+}$, $Fe^{14+}$, and $Fe^{16+}$. The dataset will also include the ratios $O^{7+}/O^{6+}$ and $C^{6+}/C^{5+}$. These data are completely unique to *Wind* and not currently publicly available. The data will be released to SPDF as CDF files.

**EPACT**

*Documentation:* The Energetic Particles: Acceleration, Composition and Transport (EPACT) investigation consists of multiple telescopes including: the Low Energy Matrix Telescope (LEMT); SupraThermal Energetic Particle telescope (STEP); and ELectron-Isotope TElescope system (ELITE). ELITE is composed of two Alpha-Proton-Electron (APE) telescopes and an Isotope Telescope (IT). IT failed early in the mission and was turned off while APE only returns two energy channels of ∼5 and ∼20 MeV protons during enhanced periods. LEMT – covering energies in the 1-10 MeV/nuc range – and STEP – measuring ions heavier than protons in the 20 keV to ∼1 MeV/nuc range – still continue to provide valuable data. These instruments have been described by *von Rosenvinge et al.* [1995]. The instrument portion of this paper is reproduced at the *Wind* project webpage (https://wind.nasa.gov). Additional instrument information is available at the instrument webpage (https://epact2.gsfc.nasa.gov/).

*Data Products:* Fluxes for a select number of ions (helium, oxygen, iron and combined CNO) in energy bins below 1 MeV/nuc and averaged over 92 seconds are publicly available for the whole mission in KP files at CDAWeb. However, the low count rates of heavy ions leads to a significant fraction of this data product being null. A systematic search for events with non-zero count rates was been undertaken, where the team identified 41 multi-day duration periods of intense particle events in the 1997–2006 time range. For these intervals, hourly omnidirectional intensity (OMN), ion sectored count (SEC), and first order ion anisotropy data were generated. These ASCII text files are publicly available at the *Wind* project webpage.

The publicly available data products are shown in Table 8.

**Table 8:** Publicly Available EPACT Data Products

| Data Product | Cadence | Coverage | Format | Location |
|---|---|---|---|---|
| KP fluxes | 92 s | 1994/11/16–2017/02/14[h] | CDF | CDAWeb[a] |
| OMN[b] | 1 hr | 41 Events | ASCII | *Wind* Project[c] |
| SEC[d] | 1 hr | 41 Events | ASCII | *Wind* Project |
| Anisotropy | 1 hr | 39 Events | ASCII | *Wind* Project |
| LEMT[f] | 1 hr | 1994/11/03–2016/12/31[h] | CDF | CDAWeb |
| LEMT[f] | 5 min | 1994/11/03–2014/09/06[h] | CDF | CDAWeb |
| APE-B[f] | 1 hr | 1994/11/03–2016/12/31[h] | ASCII | VEPO[g] |

[a] https://cdaweb.gsfc.nasa.gov; [b] omnidirectional fluxes; [c] https://wind.nasa.gov; [d] sectored counts; [e] https://omniweb.gsfc.nasa.gov; [f] omnidirectional fluxes; [g] https://vepo.gsfc.nasa.gov; [h] range at time of submission of proposal

Hourly-averaged omnidirectional particles fluxes from LEMT subsystem of the *Wind*/EPACT instrument are available from OMNIWeb (https://omniweb.gsfc.nasa.gov) and SPDF/CDAWeb. The data cover the entire mission from 3 November 1994 – 31 December 2016 and will be updated periodically. These data are also available at the Virtual Energetic Particle Observatory or VEPO (https://vepo.gsfc.nasa.gov). The data include He, C, O, Ne, Si, and Fe in seven energy bins (six for Ne) from ∼2–10 MeV/nuc. The Multi–Source Spectra Plot Interface of VEPO allows one to easily compare simultaneous measurements from other missions (e.g., ACE, STEREO, etc.). Locations of the LEMT data can be found in the Heliophysics Data Portal or HDP (http://heliophysicsdata.sci.gsfc.nasa.gov/) using the text restriction "LEMT".

*Future Data Products:* The EPACT team is working to produce data from the STEP telescope for the entire mission. The data product will include 1 hour sector-averaged and 10 min omnidirectional intensities between ∼20–2560 keV/nuc in ∼6–10 energy steps. The heavy ions included in this dataset will include H, He, CNO, NeS, and Fe. Similar to the new SMS data products, this will be unique to *Wind*.

**MFI**

*Documentation:* The *Wind* Magnetic Field Investigation (MFI) is composed of two fluxgate magnetometers located at the mid point and end of a long boom. The instrument measures DC vector magnetic fields up to a time resolution of ∼22 or ∼11 vectors/sec depending on the telemetry mode of the spacecraft. The instrument is completely described in an article by *Lepping et al.* [1995]. The instrument description sections of this paper are reproduced at the *Wind* project webpage (https://wind.nasa.gov). The data processing algorithms employed in generating the MFI data products are described by *Farrell et al.* [1995], available at the *Wind* Project webpage.

*Data Products:* The MFI team generates 3-vector magnetic fields at multiple time resolutions (e.g., 3s, 92s, etc.) with varying calibration qualities depending on the data product. Within 24 hours of measurement, the 92-second KP data is publicly available at CDAWeb. This data uses periodically updated calibration tables. Generally within ∼1–2 weeks the MFI team produces a calibrated data product that includes 3-second, 1 minute and 1 hour averages (version 3). Roughly one month after measurement, the final calibration and offsets are determined with uncertainties now reduced to a few tenths of a nT (version 4). The version 4 CDF files replace the version 3 files when uploaded to SPDF/CDAWeb. The final archival data product (version 5) requires ∼2–3 months to remove all spacecraft "noise" and other artifacts. All of these file versions have the exact same internal format.

**Table 9:** Publicly Available MFI Data Products

| Data Product | Cadence | Coverage | Format | Location |
|---|---|---|---|---|
| KP | 92 s | 2010/09/01–2017/02/14[a] | CDF | CDAWeb[b] |
| Versions 3 & 4[c] | 3 s, 1 min, 1 hr | 1994/11/16–2017/02/09[a] | CDF | CDAWeb |
| Version 5 (H0) | 3 s, 1 min, 1 hr | 1994/11/16–2017/02/09[a] | CDF | CDAWeb |
| High Res. (H2) | ∼11 or ∼22 vec/sec | 1994/11/16–2017/02/09[a] | CDF | CDAWeb |

[a] range at time of submission of proposal [b] https://cdaweb.gsfc.nasa.gov; [c] files are eventually replaced by version 5 and no longer publicly available

The publicly available data products are shown in Table 9.

The highest sample rate data (i.e., ∼11 or ∼22 vectors/sec, depending on spacecraft location relative to Earth) is kept in a separate CDF file (H2) from the lower rate data (H0) at ∼3s resolution. This is partly

due to file size differences, backwards compatibility (i.e., the ∼11 vectors/sec was never included in the H0 files), and differences in calibration efforts (e.g., spin tones and other effects not present in H0 data).

**WAVES**

*Documentation:* The *Wind* WAVES experiment is composed of three pairs of orthogonal antennas (electric fields) and a search coil magnetometer that operate as both radio receivers from ∼few Hz to ∼13 MHz and burst waveform capture time series receivers. The radio receiver array includes: the low frequency FFT receiver (FFT) from ∼few Hz to ∼11 kHz; the thermal noise receiver (TNR) from ∼4 kHz to ∼256 kHz; radio receiver band 1 (RAD1) from ∼20 kHz to ∼1040 kHz; and radio receiver band 2 (RAD2) ∼1.075–13.825 MHz. The waveform capture array contains two time domain sampler (TDS) receivers, slow (TDSS) and fast (TDSF). The TDSS receiver returns four vector fields of three magnetic(electric) and one electric(magnetic) field components at sample rates from ∼117–7500 vectors/s. The TDSF receiver returns two electric field components at sample rates from ∼1800–120000 vectors/s. The instrument is fully documented by *Bougeret et al.* [1995]. The instrument related sections of this paper are reproduced at the *Wind* project webpage (https://wind.nasa.gov). Some additional documentation exists also at the WAVES instrument webpage (https://solar-radio.gsfc.nasa.gov/wind/index.html). The content and format of the various WAVES data products are also described on the instrument webpage.

*Data Products:* As most other *Wind* instruments, WAVES also produces a KP data product that is immediately publicly available at CDAWeb. The WAVES KP data contains 3-minute averages of the electric field intensities at 76 log-spaced frequencies and electron density estimates based on neural network determined electron plasma frequency values. The WAVES team produces 1 min resolution radio data, within ∼1 week of observation, as a frequency vs. time intensity product and distributes these data on both the instrument webpage and CDAWeb. The ∼7–10 second total electron density estimates from the upper hybrid line are also made available on CDAWeb.

The WAVES team also maintains a Type II/IV catalog on the instrument website and a similar list can be found at the CDAW Data Center (https://cdaw.gsfc.nasa.gov/CME_list/radio/waves_type2.html) or through a link on the *Wind* project webpage.

**Table 10:** Publicly Available WAVES Data Products

| Data Product | Cadence | Coverage | Format | Location |
|---|---|---|---|---|
| KP | 3 min | 1994/11/10–2017/02/14[g] | CDF | CDAWeb[a] |
| TNR[b], Rad1, Rad2[c] | 1 min | 1994/11/10–2017/02/14[g] | ASCII, IDL Save | CDAWeb, WAVES[d] |
| High Res. $n_e$[e] | 7-10 s | 1994/11/10–2017/02/15[g] | CDF | CDAWeb |
| Radio Plots | 1 min | 1994/11/10–2017/02/15[g] | PNG, PDF | WAVES |
| Dust Impacts[f] | N/A | 1995/01/01–2015/12/31 | CDF | CDAWeb |

[a] https://cdaweb.gsfc.nasa.gov; [b] Thermal Noise Receiver; [c] Radio Receiver Band 1, 2;
[d] https://solar-radio.gsfc.nasa.gov/wind/index.html; [e] electron number density; [f] dust impact database;
[g] range at time of submission of proposal

The publicly available data products are shown in Table 10.

*New Data Products:* A recently available product is the dust impact database produced by David Malaspina (PI) and Lynn. B. Wilson III (Co-I) for the WAVES–TDSF waveform captures. The database is publicly available on CDAWeb in CDF file format. The dataset includes the date and time, orientation and location of the spacecraft, impact location on the spacecraft body, dust signal type, etc. The details of the dataset are described in *Malaspina and Wilson III* [2016] and very detailed metadata can be found at CDAWeb.

*Future Data Products:* The WAVES team is nearly ready to release all TDSS and TDSF events for the entire mission for final archive to SPDF/CDAWeb. The data products will be provided in CDF format and released for public use on CDAWeb. The team has already produced a first version of the data product with successful test results for ISTP (International Solar-Terrestrial Physics) compatibility from the SPDF team. The WAVES team is currently finalizing the software for automated production.

**KONUS and TGRS**

The KONUS and TGRS $\gamma$-ray instruments are not maintained by heliophysics. Their data production and data distribution is completely handled by the astrophysics division. Description of the instruments and links to their data products can be found at:
https://heasarc.gsfc.nasa.gov/docs/heasarc/missions/wind.html; and

https://heasarc.gsfc.nasa.gov/w3browse/all/ipngrb.html.

***Wind* and VHO**

Members of the *Wind* instrument teams have taken leadership roles in the development of the Virtual Heliospheric Observatory (VHO) (https://vho.nasa.gov). Aside from assuring that the various data products are publicly open, the most effort went into the generation of SPASE dictionary based and VHO compliant metadata. In fact, the first *Wind* data product metadata files have been used to refine the SPASE dictionary for fields and particles data. Currently, all primary *Wind* data products are fully searchable via the VHO.

## Acronyms and Initialisms

3D . . . . . three-dimensional

3DP . . . . . Three-Dimensional Plasma and Energetic Particle Investigation (*Wind*/3DP)

ACE . . . . . Advanced Composition Explorer

ACR . . . . . Anomalous Cosmic Ray

APE . . . . . Alpha-Proton-Electron telescope (part of *Wind* EPACT/ELITE)

ARTEMIS . . . . . Acceleration, Reconnection, Turbulence and Electrodynamics of the Moon's Interaction with the Sun

AU . . . . . Astronomical Unit

CAP . . . . . Command and Attitude Processor

CCMC . . . . . Coordinated Community Modeling Center

CDAWeb . . . . . Coordinated Data Analysis Web

CIR . . . . . Corotating Interaction Region

CME . . . . . Coronal Mass Ejection

CRIS . . . . . Cosmic-Ray Isotope Spectrometer

DiP . . . . . Distortion Parameter

DSA . . . . . Diffusive Shock Acceleration

DSCOVR . . . . . Deep Space Climate Observatory

DSN . . . . . Deep Space Network

DTR . . . . . Digital Tape Recorder

E/PO . . . . . Education and Public Outreach

EESA . . . . . Electron Electrostatic Analyzer (*Wind*/3DP)

EH . . . . . Electron Hole

ELITE . . . . . Electron-Isotope Telescope system (*Wind*/EPACT)

EPACT . . . . . Energetic Particles: Acceleration, Composition, and Transport (APE-ELITE-IT-LEMT package on *Wind*)

EPAM . . . . . Electron, Proton and Alpha Monitor

EPP . . . . . Electron Pitch-angle distribution Parameter

ESA (agency) . . . . . European Space Agency

ESA (detector) . . . . Electrostatic Analyzer

ESW . . . . . Electrostatic Solitary Wave

FAB . . . . . Field-Aligned (ion) Beam

FC . . . . . Faraday Cup

FOT . . . . . Flight Operations Team

FR . . . . . Flux-Rope

FTE . . . . . Full Time Equivalent

FTP . . . . . File Transfer Protocol

GCN . . . . . Gamma-ray Coordinates Network

GeV . . . . . Giga-electron volt

GF . . . . . Giant Flare

GGS . . . . . Global Geospace Science

GLE . . . . . Ground-Level Events

GOES . . . . . Geostationary Operational Environmental Satellites

GRB . . . . . Gamma Ray Burst

GSFC . . . . . Goddard Space Flight Center

GUI . . . . . Graphical User Interface

HDP . . . . . Heliophysics Data Portal

HET . . . . . High-Energy Telescope

HETE-2 . . . . . High Energy Transient Explorer-2

HGO . . . . . Heliophysics Great Observatory

HI . . . . . Heliospheric Imagers

HK . . . . . House Keeping

HSO . . . . . Heliophysics System Observatory

HTR . . . . . High Time Resolution

IBEX . . . . . Interstellar Boundary Explorer

ICME . . . . . Interplanetary Coronal Mass Ejection

ICW . . . . . Ion Cyclotron Wave

IMAP . . . . . Interstellar MApping Probe

IMF . . . . . Interplanetary Magnetic Field

IMP . . . . . Interplanetary Monitoring Platform (spacecraft)

IMPACT . . . . . In-situ Measurements of Particles and CME Transients (suite)

INTEGRAL . . . . . INTErnational Gamma-Ray Astrophysics Laboratory

IP . . . . . Interplanetary

IPD . . . . . Interplanetary Dust

IPM . . . . . Interplanetary Medium

IPN . . . . . Interplanetary GRB Network

ISD . . . . . Interstellar Dust

ISS . . . . . International Space Station

ISTP . . . . . International Solar-Terrestrial Physics

iSWA . . . . . integrated Space Weather Analysis system

IT (detector) . . . . . Isotope Telescope (part of *Wind* EPACT/ELITE)

ITOS . . . . . Integrated Test and Operations System

keV . . . . . kilo-electron volt

KH . . . . . Kelvin-Helmholtz

KONUS . . . . . Gamma-Ray Spectrometer

KP . . . . . Key Parameter

LASCO . . . . . Large Angle and Spectrometric COronagraph

LEMT . . . . . Low Energy Matrix Telescopes (*Wind*/EPACT)

LET . . . . . Low Energy Telescope

LIGO . . . . . Laser Interferometer Gravitational-Wave Observatory

LWS . . . . . Living With a Star

LZ . . . . . Level Zero

MAG . . . . . magnetic field experiment

MASS . . . . . high-resolution mass spectrometer (*Wind*/SMS)

MAVEN . . . . . Mars Atmosphere and Volatile EvolutioN mission

MC . . . . . Magnetic Cloud

MESSENGER . . . . . Mercury Surface Space Environment Geochemistry and Ranging

MeV . . . . . Mega-electron volt

MHD . . . . . Magnetohydrodynamic

MMOC . . . . . Multi-Mission Operations Center

MMS . . . . . Magnetospheric Multi-Scale NASA STP mission

MO . . . . . Magnetic Obstacle

MOMS . . . . . Mission Operations and Mission Services

MOVE . . . . . Mission Operations Voice Enhancement

NASA . . . . . National Aeronautics and Space Administration

OMNI . . . . . omnidirectional or dataset on CDAWeb

PAD . . . . . Pitch-Angle Distribution

PESA . . . . . Ion Electrostatic Analyzer (*Wind*/3DP)

PLASTIC . . . . . PLAsma and SupraThermal Ion Composition

PMS . . . . . Planar Magnetic Structure

PWG . . . . . Polar-Wind-Geotail ground system

RBSP . . . . . Radiation Belt Storm Probes (now *Van Allen Probes*)

RHESSI . . . . . Reuven Ramaty High Energy Solar Spectroscopic Imager

SC . . . . . Solar Cycle

SDO . . . . . Solar Dynamics Observatory

SECCHI . . . . . Sun-Earth Connection Coronal and Heliospheric Investigation

SEP . . . . . Solar Energetic Particle

SEPT . . . . . Solar Electron and Proton Telescope

SEU . . . . . Single Event Upset

SGR . . . . . Soft Gamma Repeater

SHH . . . . . soft-to-hard-to-harder (i.e., change for X-ray spectra)

SIR . . . . . Stream Interaction Region

SIS . . . . . Solar Isotope Spectrometer

SIT . . . . . Suprathermal Ion Telescope

SLAMS . . . . . Short Large Amplitude Magnetic Structures

SMD . . . . . Science Mission Directorate

SMS . . . . . Solar Wind and Suprathermal Ion Composition Experiment (SWICS-MASS-STICS package on *Wind*)

SOHO . . . . . SOlar and Heliospheric Observatory

SolO . . . . . Solar Orbiter mission

SPASE . . . . . Space Physics Archive Search and Extract

SPDF . . . . . Space Physics Data Facility

SPP . . . . . Solar Probe Plus mission

sps . . . . . samples per second

SSMO . . . . . Space Science Mission Operations

SSN . . . . . Sun Spot Number

SST . . . . . Solid-State (semi-conductor detector) Telescope (*Wind*/3DP)

ST . . . . . Small Transient

STE . . . . . SupraThermal Electron instrument

STEP . . . . . SupraThermal Energetic Particle Telescope (*Wind*/EPACT)

STEREO . . . . . Solar-Terrestrial Relations Observatory

STICS . . . . . SupraThermal Ion Composition Spectrometer (*Wind*/SMS)

SWE . . . . . Solar Wind Experiment

SWEA . . . . . Solar Wind Electron Analyzer

SWEPAM . . . . . Solar Wind Electron Proton Alpha Monitor (ACE)

SWICS . . . . . Solar Wind Ion Composition Spectrometer

SWIMS . . . . . Solar Wind Ion Mass Spectrometer

TD . . . . . Tangential Discontinuity

TDS . . . . . Time Domain Sampler (*Wind*/WAVES)

TDSF . . . . . Time Domain Sampler Fast (*Wind*/WAVES)

TDSS . . . . . Time Domain Sampler Slow (*Wind*/WAVES)

TGRS . . . . . Transient Gamma-Ray Spectrometer

THEMIS . . . . . Time History of Events and Macroscale Interactions during Substorms

THOR . . . . . Turbulence Heating ObserveR

TNR . . . . . Thermal Noise Receiver (e.g., part of *Wind*/WAVES)

TPOCC . . . . . Transportable Payload Operations Control Center

TRACE . . . . . Transition Region And Coronal Explorer

TUA . . . . . Tape Unit A

TUB . . . . . Tape Unit B

ULEIS . . . . . Ultra Low Energy Isotope Spectrometer

VDS . . . . . Voice/Video Distribution System

VEIS . . . . . Vector Ion-Electron Spectrometers (*Wind*/SWE)

VEPO . . . . . Virtual Energetic Particle Observatory

VEX . . . . . Venus EXpress

VHO . . . . . Virtual Heliophysics Observatory

VWO . . . . . Virtual Waves Observatory

WYE . . . . . Work Year Equivalent

## Budget Spreadsheet

**Table 11:** Wind *Senior Review Budget Spreadsheet*